University of Minnesota
St. Anthony Falls Hydraulic Laboratory

Project Report No. 348

Methane Sampling Technique and the Measurement of Plunge Pool Impact on Gas Transfer Rates at Low-Head Hydraulic Structures

by

David E. Hibbs and John S. Gulliver
St. Anthony Falls Hydraulic Laboratory
University of Minnesota
Minneapolis, Minnesota

and

John P. McDonald
Zenk Read Trygstad and Associates, Inc.
Albert Lea, Minnesota

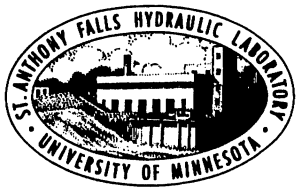

DRAFT REPORT
Prepared for

U.S. ARMY ENGINEER
WATERWAYS EXPERIMENT STATION

November 1993
Minneapolis, Minnesota

DRAFT REPORT TO THE U.S. ARMY ENGINEER, WATERWAYS EXPERIMENT STATION

Methane Sampling Technique and the Measurement of Plunge Pool Impact on Gas Transfer Rates at Low-Head Hydraulic Structures

by

David E. Hibbs[1], John S. Gulliver[2]
and John P. McDonald[3]

November, 1993

---

[1]Graduate Research Assistant, University of Minnesota, St. Anthony Falls Hydraulic Laboratory, Minneapolis, MN 55414 (612) 627-4010.

[2]Associate Professor, Department of Civil & Mineral Engineering, St. Anthony Falls Hydraulic Laboratory, (612) 627-4600.

[3]Environmental Engineer, Zenk Read Trygstad and Assoc., Inc., Albert Lea, MN, 56007, (507) 373-0689.

TABLE OF CONTENTS

LIST OF FIGURES

LIST OF TABLES

LIST OF PHOTOGRAPHS

ACKNOWLEDGEMENTS

Funding for the research was provided by the Reservoir Water Quality Branch of the Hydraulics Laboratory, U.S. Army Engineer Waterways Experiment Station, and by the Minnesota State Legislature, ML 1989, Chap. 335, Sec. 29, Subd. 82, as recommended by the Legislative Commission on Minnesota Resources. Thanks to Steven C. Wilhelms for allowing us to use his air entrainment data, and for general discussions on the topic. Thanks also to Professor Michael J. Semmens for the availability of the gas chromatograph and to John R. Thene for advice on developing the headspace technique for methane.

I. INTRODUCTION

Hydraulic structures have a large impact on the amount of dissolved gases in a river system. Even though the water passes over the structure for only a short time, the water flowing over a spillway or weir entrains air bubbles, creating significantly more air-water surface area for gas transfer. In addition, the high turbulence that occurs at most hydraulic structures will increase the transfer rate coefficients. The same quantity of gas transfer that normally would occur in several miles in a river can occur at a hydraulic structure.

The transfer of oxygen from the atmosphere to the water is often of interest, therefore it seems logical to directly measure oxygen transfer. However, there are some problems associated with the measurement of dissolved oxygen (DO) concentration. If the DO level is close to saturation (within approximately 2.5 mg/ℓ), the tremendous uncertainty associated with the current measurement techniques makes the estimation of gas transfer useless (Gulliver and Wilhelms, 1992). Also, if the reservoir is stratified, it is difficult to predict withdrawal from the various layers with the required precision, and usually impossible to sample at the spillway crest (Gulliver and Rindels, 1993). Because the required field conditions for accurate DO measurement often do not occur, other measurement techniques, such as the tracer technique are used.

The first tracer technique for reaeration rate measurement in open channels was introduced by Tsivoglou (1968). The basic assumption behind Tsivoglou's technique is that the ratio between the desorption of the tracer gas and the absorption rate of oxygen is a constant. The ratio of tracer gas transfer rate to the oxygen transfer rate can be determined through laboratory experiments involving the simultaneous transfer of both gases. Since the driving force of gas transfer is the partial pressure difference between the concentration in equilibrium with the atmosphere,which is linearly proportional to the partial pressure in the atmosphere, and that dissolved in water, tracers that have no significant atmospheric component should be chosen. Thus, measurements can be made with a tracer saturation concentration of essentially zero. Tsivoglou injected radioactive krypton-85 into a river and measured its desorption along the river reach. Tsivoglou's technique worked rather well, but required the use of radioactive materials.

Rathbun et al. (1978) modified Tsivoglou's method by substituting propane and ethylene in place of krypton-85 to avoid the use of radioactive materials. The assumptions made were similar to Tsivoglou's with changes made for the desorption rates of propane and ethylene. One major restriction is that measurable quantities of the tracer could only be obtained by bubbling the gas through pneumatic

diffusers, requiring additional field equipment. A more extensive review of gas tracer techniques is given in McCutcheon (1989).

Thene and Gulliver (1990) developed a headspace measurement technique for propane gas tracer and subsequently found measurable amounts of naturally occurring methane in the samples. The unanticipated quantities of methane held promise for the use of methane as a tracer gas. Methane is produced in the sediments as a by-product of the anaerobic decomposition of organic materials. No injection of artificial tracer gases is needed, which can be a substantial savings in cost and effort at the larger hydraulic structures. In addition, the uncertainty associated with the transverse mixing of the injected tracers is eliminated. The technique is more effective at low-head structures since stratification of methane has been observed at higher-head structures(Wilhelms, et al, 1993).

McDonald and Gulliver (1992) measured oxygen and methane transfer over several hydraulic structures. After correction for diffusivities, oxygen and methane transfer efficiencies were found to be comparable at a given structure except when the entrained air bubbles were pulled to a depth in the tailwater. Because of the high static and dynamic pressures that a bubble experiences in a plunging jet flow, the concentration of atmospheric gases will be greater in the bubble than at the water surface. The rate of gas transfer will correspondingly be higher for oxygen and nitrogen due to the higher saturation concentration of the water in contact with the bubble. This problem was delineated by determining an "effective" saturation concentration from oxygen and methane measurements that incorporates the higher pressure exerted on bubbles in the plunge pool.

This paper describes the development and testing of the methane tracer technique for determining gas transfer rates at low-head hydraulic structures. The effect of the plunge pool on the gas transfer rate is also examined by comparing the tracer gas transfer rate to the rate for oxygen and nitrogen.

II. METHANE IN THE WATER COLUMN

Process of Methane Production

Methane is produced as a by-product of the anaerobic decomposition of organic material. Methanogenesis is the terminal process in a chain of decomposition processes in the anaerobic hypolimnion and represents a major mechanism by which carbon leaves the sediments (Strayer and Tiedje, 1978). Methane transfer out of the sediments and hypolimnia is by vertical diffusion and, if enough methane is produced, by bubble ebullion.

Methane production is a two-stage process. In the first stage a group of faculative and obligate bacteria, termed acid formers, turn proteins, carbohydrates and fats into fatty acids by hydrolysis and fermentation. Methane producing bacteria then convert these acids into methane. Some alcohols from carbohydrate fermentation can also be converted to methane by methane producing bacteria (Wetzel, 1975).

The concentration of acetate, H_2, and CO_2, the major substrates for methane production, are highly variable and are dependent upon the organic material. Acetate is the preferred substrate for methanogenesis at low partial pressures of H_2. As the partial pressure of hydrogen rises, bicarbonate is the preferred substrate.

The reaction of methane production from the reduction of carbon dioxide is given as:

$$CO_2 + 8H^+ \rightarrow CH_4 + 2H_2O \qquad (1)$$

In the second process, the production of methane from acetic acid can be shown as:

$$CH_3COOH \rightarrow CH_4 + CO_2 \qquad (2)$$

The later process is thought to produce about 70% of methane in the water column with much of the remainder coming from the reduction of CO_2. Fermentation of other acids are of less importance.

Bacteria that produce methane are strictly anaerobic. Even slight traces of oxygen are toxic to these bacteria. They consist of four major genre: rod-shaped, non-sporiferous Methanobacterium, rod-shaped sporiferous Methanobacillus, the spherical Methanococcus and Methanosurcina. These bacteria have a wide temperature range for growth. Zeikus and Winfrey (1976) found methanogenesis occurring at temperatures from 4°C to 45°C, although the rates were highly temperature dependent. A change of 12°C in the temperature of the sediments during the change of seasons was associated with a 100 to 400 fold increase in the rate of methanogenesis.

Methanogenesis is severely limited by sulfate reduction. Waters that have high methane concentration generally have low

sulfate concentrations and vice versa. This is because the sulfate reducing bacteria out compete the methane producing bacteria for H_2 and acetate, both precursors of methane production (Abram and Nedwell, 1978). The reduction of sulfate in the sediments is described by

$$SO_4^- + 9H^+ \rightarrow HS^- + 4H_2O \quad (3)$$

Millimolar quantities of sulfate will inhibit methane production. The sulfate reducing bacteria have a higher affinity for hydrogen and acetate than methane producing bacteria thus keeping the pool of these substrates at a level too low to be used by the methane producing bacteria (Lovley et al., 1982). In addition, thermodynamic calculations can be used to predict the exclusion of methane production in sulfate containing sediments.

Very little of the methane produced in lakes or reservoirs escapes to the atmosphere because of the relatively quiescent nature of the waterbody or the low turbulence intensities near the water surface. Rudd (1979) measured evasion rates of 5% of the total methane produced. Fallon et al (1980) measured an evasion rate of 9% in Lake Mendota, Wisconsin. The small evasion rates are due to the presence of methane oxidizing bacteria, with aerobic methane oxidation that is given by:

$$5CH_4 + 8O_2 \rightarrow 2(CH_4) + 3CO_2 + 8H_2O \quad (4)$$

Because the residence time over a hydraulic structure is short it is assumed that no significant methane oxidation occurs over the time it takes a methane molecule to pass through a structure. For example, while the half-life of methane over a structure is on the order of seconds due to the large surface area and high turbulence of the flow, the half-life of methane in the river and reservoir is on the order of hours. Therefore, it is assumed that the only pathway for a methane molecule to leave the water column during the retention time over a structure is by evasion to bubbles or the atmosphere.

Methane Concentrations

Methane was sampled in a number of reservoirs to estimate how often one could expect relatively high (above the limit of quantification, LOQ) methane concentrations. Methane concentrations were sampled in seven reservoirs during fall, winter and spring, and in all but one reservoir they were well above our current LOQ of 0.3 $\mu g/\ell$ (the LOQ is developed in Section VI). Sample methane isopleths obtained from the Coon Rapids Dam are shown in Figs. 1 and 2. The concentrations varied from 119 to 4 $\mu g/\ell$ in the six reservoirs. All six reservoirs were fairly shallow, with depths ranging from 3m

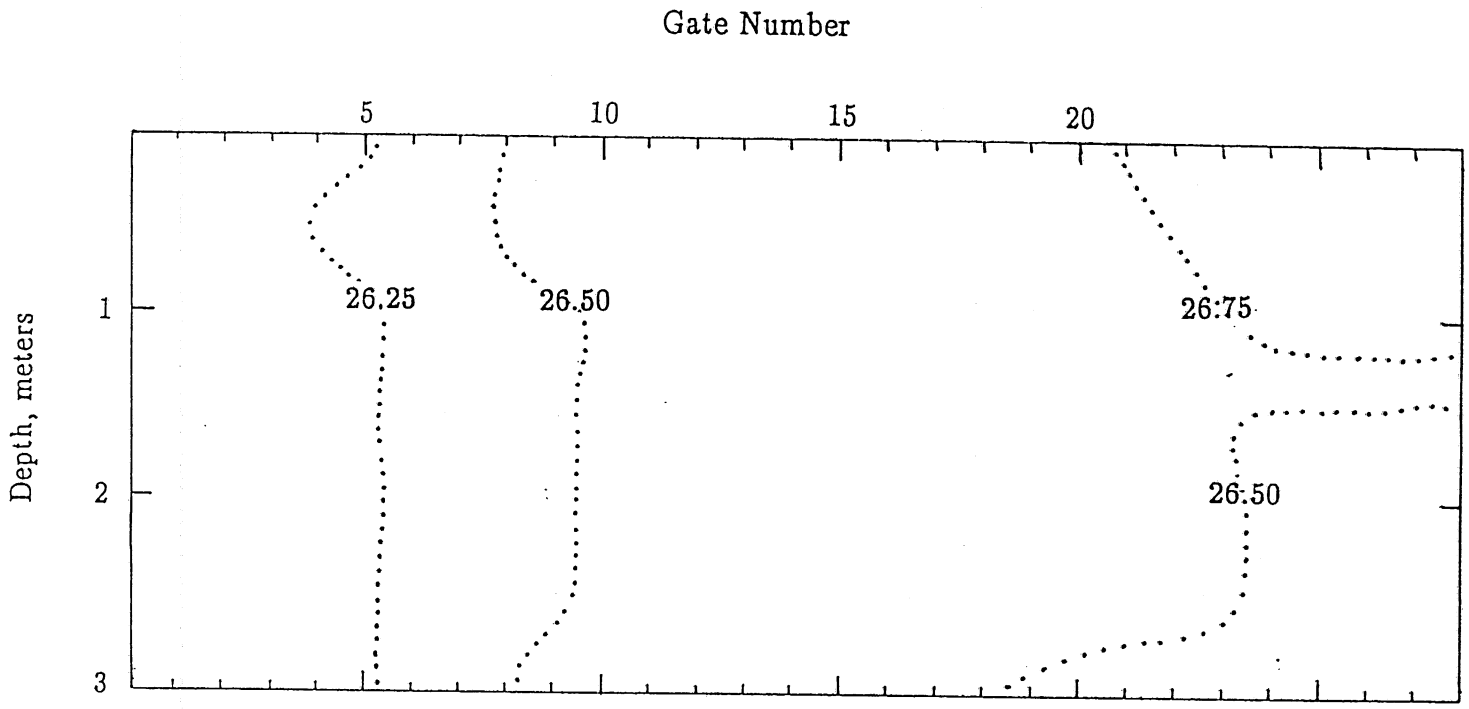

Figure 1 - Methane isopleth from Coon Rapids Dam 8/1/89

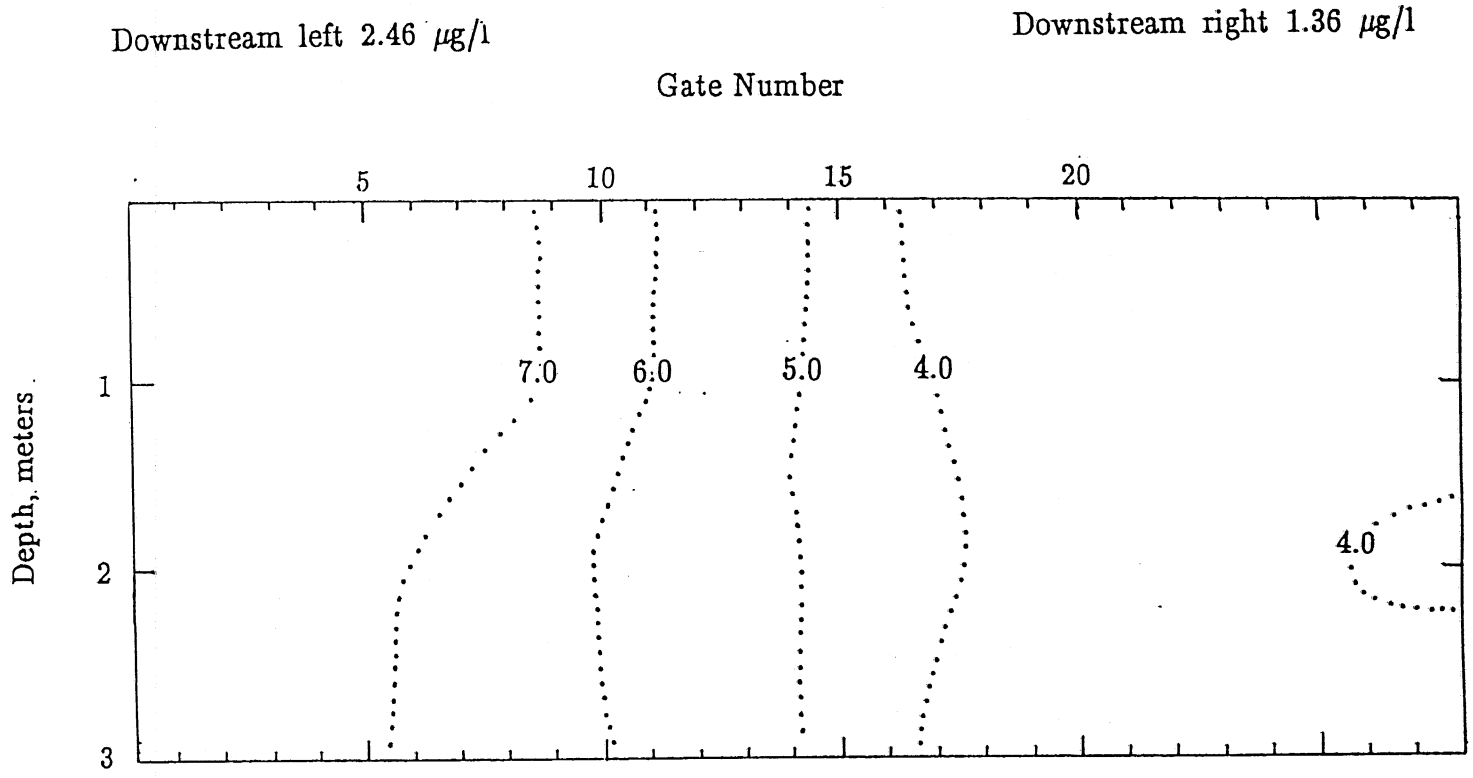

Figure 2 - Methane isopleth from Coon Rapids Dam 10/6/89

(10 ft) to 9m (30 ft). The exception was one relatively deep (18m or 60 ft) reservoir with a methane concentration of approximately 0.5 $\mu g/\ell$. This reservoir was held back by a hollow gravity dam, and the leakage into the hollow center had a strong hydrogen sulfide smell. As mentioned previously, methanogenesis is severely limited by sulfate production, which is believed to be occurring in this reservoir.

Methane was supersaturated at all locations sampled . This agrees with results from de Angelis and Lilley (1987). The bacterial oxidation of methane and methane evasion rates (i.e. the pathways by which methane escapes from the water column) are inadequate to remove all the methane from these reservoirs.

Methane concentrations were also not highly stratified in the shallow reservoirs except under ice cover, where methane was found at much larger concentrations just under the ice than near the sediments at many sites. This may be due to methane bubbles rising from the sediments. The ice cover would block methane evasion to the atmosphere, leaving the water just under the ice at a higher concentration. Another thought is that perhaps the ice itself contains a high amount of methane, and the water in contact with the melting ice in early spring will also have a correspondingly high methane concentration. Methane stratification may also be due to inputs into the river/reservoir.

Results of these field measurements show that under conditions of thermal stratification in reservoirs, methane will also be stratified, although not as strongly as oxygen. The highly active photic zone near the reservoir surface will enhance the naturally occuring oxygen stratification. Such is not the case for methane. The primary service that methane can provide as a gas tracer, however, would be as a substitute for O_2 and N_2 transfer at structures associated with non-stratified reservoirs, when the two gases are close to saturation. Methane will likely be present at measurable quantities and will be well above saturation.

III. THEORY AND ANALYSIS

Gas Transfer at Hydraulic Structures

Gas transfer is typically described as a first-order process in which the rate of change of the gas concentration in the water is linearly dependent a concentration difference or driving force. The flux of any volatile dissolved chemical across an air-water interface may be given by the equation:

$$F=\frac{V}{A}\frac{dC}{dt}=K_L\left(\frac{C_a}{H}-C\right) \qquad (5)$$

where F is mass flux rate per unit surface area, K_L is the liquid film coefficient, C_a is the concentration of the chemical in the air, C is the concentration of the dissolved chemical in the water, A is the air-water interface surface area, V is the control volume over which C and A are measured, t is time, and H is Henry's law constant, an equilibrium partitioning constant. C_a/H is often called the saturation concentration, C_s. Because the chemicals oxygen, nitrogen, and gas tracers of interest are volatile, only the liquid phase resistance to transfer (K_L) is considered. The gas phase resistance is much less than the liquid phase resistance, and is therefore neglected.

For transfer at a hydraulic structure, Eq. 5 can be integrated from upstream of the structure to downstream of the structure, resulting in an equation for transfer efficiency (Gulliver and Rindels, 1993):

$$E=\frac{C_d-C_u}{C_s-C_u}=1-\exp\left[-\int_{t_u}^{t_d}K_L\frac{A}{V}dt\right] \qquad (6)$$

where the subscripts 'u' and 'd' refer to measurement locations upstream and downstream of the structure, respectively. A transfer efficiency of 1.0 means the full gas transfer up to the saturation value has occurred. No gas transfer would correspond to E = 0.0. A transfer efficiency of greater than 1.0 means the gas has become supersaturated downstream. For gases which do not have appreciable concentrations in the atmosphere (like methane), C_a and C_s are close to zero, and transfer efficiency can be written as:

$$E=\frac{C_u-C_d}{C_u} \quad (non\text{-}atmospheric\ gas\ transfer) \qquad (7)$$

Indexing Gas Transfer

Gulliver et al. (1990) developed an indexing relationship to directly compare liquid phase controlled transfer efficiencies, such as those considered herein, at hydraulic structures. This relationship can be used to index transfer measurements to a common temperature and a common gas (most often oxygen is used in gas transfer measurements). The relationship is given as:

$$E_{iO}=1-(1-E_m)^{1/f_i} \quad (8)$$

where E_m is the measured transfer efficiency, i.e. the transfer efficiency of methane, and E_{iO} is the equivalent transfer efficiency of the index gas , i.e. oxygen, at the index temperature. The parameter f_i is given as

$$f_i=f_g f_T \quad (9)$$

where f_g is the diffusivity correction and f_T is the temperature correction, approximated by a curve fit to the original equation as:

$$f_T = 1.0 + 0.02103(T-20) + 8.261\times10^{-5}(T-20)^2 \quad (10)$$

where T is the temperature in °C. If the methane transfer measurements are made at the index temperature, no temperature indexing is needed and f_t is set equal to 1. The parameter f_g may be determined from the parametric relationship given by Hanratty (1991) and Rathburn (1990) to be:

$$f_g=\left[\frac{D}{D_o}\right]^{1/2} \quad (11)$$

where D is the diffusivity of the measured compound, methane, and D_o is the diffusivity of oxygen. Rathbun (1990) and Gulliver et al. (1990) give techniques to estimate D for various compounds. The diffusivity of methane in water was researched by Thene and Gulliver (1990) who searched Chemical Abstracts from 1965 through 1986 and found 14 measured diffusivities with a mean value of 1.69×10^{-9} m^2/sec at 20°C. The diffusivity of oxygen (2.18×10^{-9} m^2/sec) and Eq. 11 were then used to compute an f_g value of 0.88 for the indexing of methane transfer measurements to oxygen and vice-versa.

Comparison of Oxygen and Methane Transfer Efficiencies

Simultaneous oxygen and methane measurements allow for the comparison of their transfer efficiencies. Fig. 3 shows the measured oxygen transfer efficiencies plotted against the methane transfer efficiencies indexed to oxygen for 5 low-head

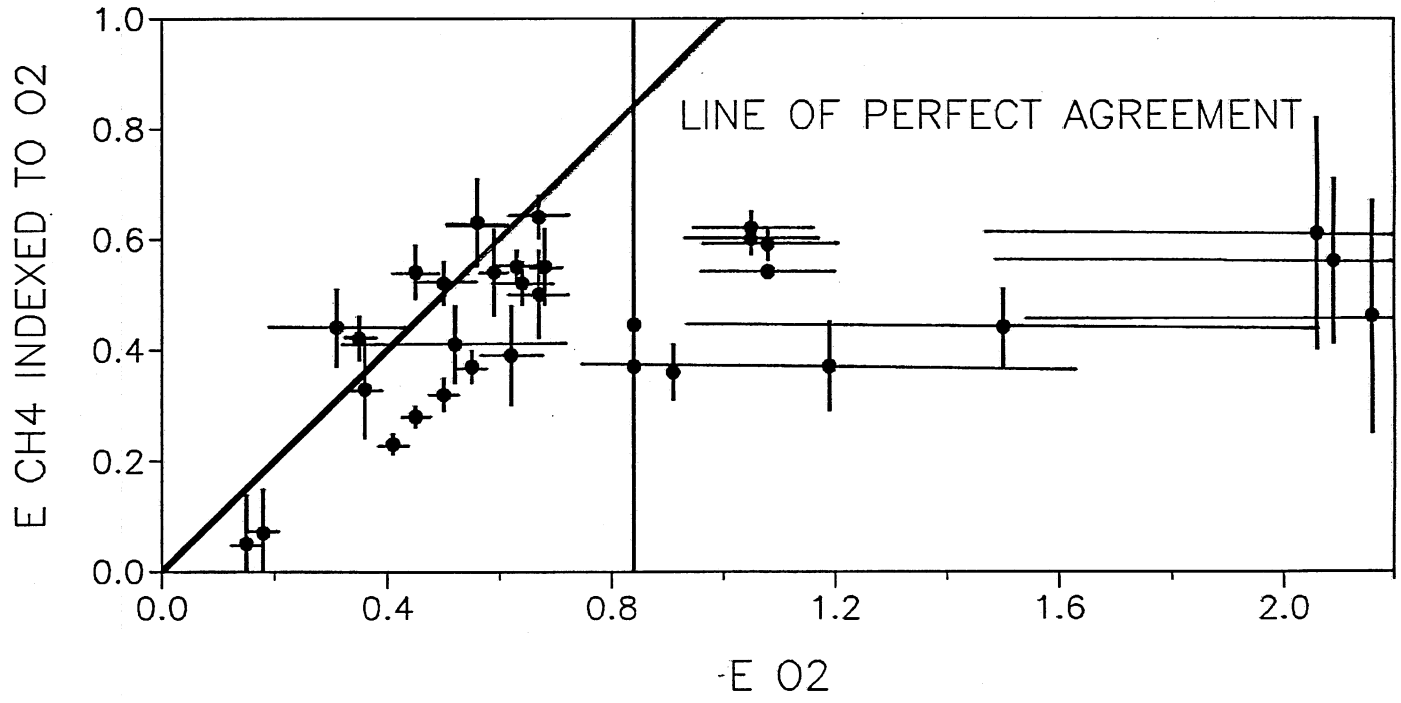

Figure 3 - Oxygen transfer efficiency versus methane transfer efficiency indexed to oxygen

structures. The oxygen transfer efficiency measurement was generally equal to or higher than the methane transfer efficiency, after indexing to an equivalent oxygen transfer, indicating a discrepancy between the two simultaneous measurements.

One possible cause of this discrepancy could be that the indexing between methane and oxygen transfer was incorrect. There is some debate over the power to be applied to the diffusivity ratio, which some have said should be 2/3 rather than 1/2 at low turbulence levels. Aside from the fact that flow at prototype hydraulic structures is highly turbulent, this difference in power would not have a significant effect on f_g. The use of a incorrect f_g could not account for the variations in inequity between indexed methane and measured oxygen transfer efficiencies given in Fig. 3. It would simply bias the results to one side or the other of perfect agreement.

A more likely cause of the incongruency of the methane and oxygen transfer efficiencies is due to the effect of tailwater on gas transfer. As illustrated in Fig. 4, the plunging water jet at the surface will carry entrained air bubbles to some depth. The hydrostatic force of the water column will result in a greater pressure inside these entrained bubbles as the bubbles are pulled deeper. Additionally, as the jet reaches the bottom of the plunge pool, some force acts on the flow to remove the vertical component of velocity, deflecting the spillway jet horizontally out of the plunge pool. This force also increases the pressure on the entrained bubbles. The increased pressures yield a greater partial pressure of oxygen in the bubbles, and hence, an increased saturation concentration than would occur at atmospheric pressure.

This phenomena increases the transfer of atmospheric gases such as oxygen and nitrogen, since the bubbles will contain significant amounts of these gases. However, for methane and other gases which do not have significant atmospheric concentrations, the hydrostatic and dynamic forces acting in the plunge pool will not increase the gas transfer rate since the partial pressures of these gases in a bubble will be close to zero in most cases. This will be shown for one typical structure later in the paper.

The integration of Eq. 5 to result in Eq. 6 assumed that the saturation concentration was constant. For methane transfer, the saturation concentration is essentially zero regardless of the pressure within the bubble, and therefore Eq. 6 is applicable. However, for atmospheric gases, this is obviously not true. Thus, an oxygen transfer efficiency measurement should assume a saturation concentration that corresponds to pressures somewhat higher than atmospheric. Determination of this pressure and corresponding saturation concentration is one of two primary objectives of this paper. The primary justification is that when a tracer, such as

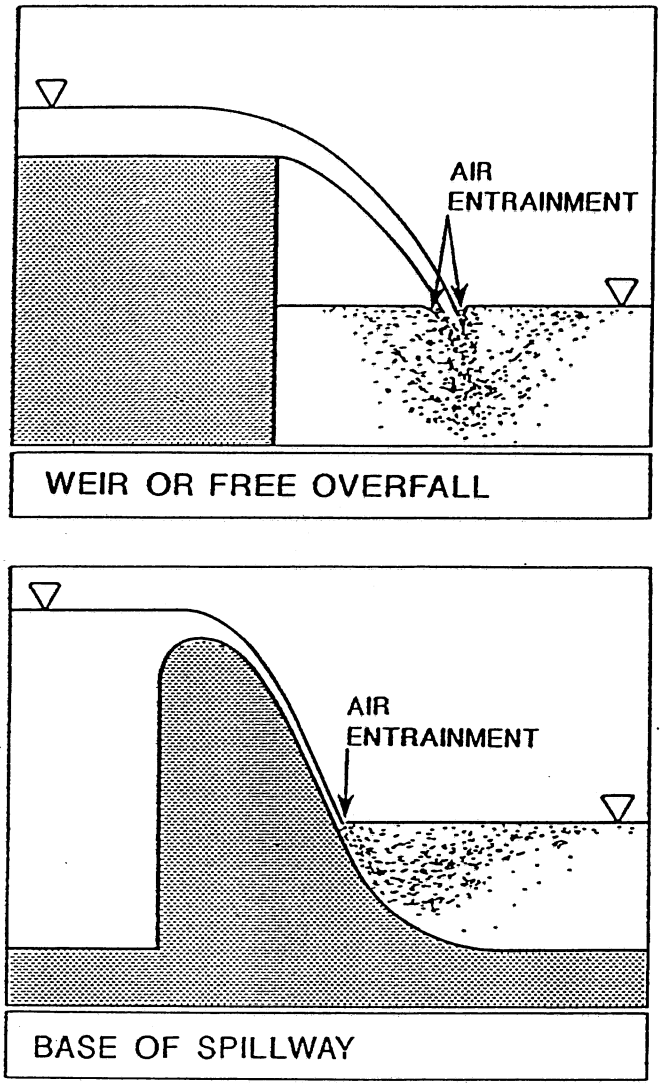

Figure 4 - Air entrainment at plunge pool surface

methane, is being used to predict an oxygen or nitrogen transfer efficiency, or when the oxygen or nitrogen transfer efficiency is being used to predict the transfer of other non-atmospheric gases, substantial errors could result. In addition, accurate prediction of oxygen and nitrogen transfer at hydraulic structures with a plunge pool is not possible without some quantification of this tailwater effect (Johnson, 1984). A technique is therefore needed to adjust for the higher pressure that the entrained bubbles experience in the tailwater pool of a hydraulic structure.

Effective Saturation Concentration and Effective Bubble Depth

The technique used to adjust for the higher pressure that the entrained bubbles experience in the plunge pool assumes that methane and either oxygen or nitrogen concentration measurements have been made at the structure. The process is then to 1) measure the methane transfer efficiency, E_m, of the structure using Eq. 7; then 2) index the methane transfer efficiency to an oxygen or nitrogen transfer efficiency with Eq. 8; and then 3) use the upstream and downstream dissolved oxygen (DO) or dissolved nitrogen measurements with the indexed transfer efficiency to compute an "effective" saturation concentration for oxygen or nitrogen, C_{se}:

$$C_{se}=\left[\frac{C_d-C_u}{E_{io}}\right]+C_u \qquad (12)$$

where E_{io} is the measured methane transfer efficiency indexed to an oxygen or nitrogen transfer efficiency and C_u and C_d are the measured DO or dissolved nitrogen concentrations upstream and downstream, respectively. The effective saturation concentration is therefore a mean of the oxygen or nitrogen saturation concentrations that the bubbles experience, weighted by their impact on gas transfer. This weighted mean saturation concentration is not determined by following bubble paths through a plunge pool, but is simply inferred from simultaneous methane and oxygen or nitrogen concentration measurements.

The effective saturation concentration can be expressed as an "effective depth", or the depth at which a bubble would be held under hydrostatic pressure to have the same equilibrium concentration as the effective saturation concentration. This depth could be compared to tailwater depth, specific discharge, head, etc., at given structures. It will be used for comparison to these parameters because of the perspective it gives relative to tailwater depth. The effective depth is computed as:
where D_{eff} is the effective bubble depth (m or ft), C_{se} is the effective saturation concentration of oxygen or nitrogen (mg/ℓ) from Eq. 12, H is Henry's Law coefficient for oxygen or

$$D_{eff}=K_p\left(\frac{C_{se}\cdot H}{comp}-P_{atm}\right) \quad (13)$$

nitrogen (atm ℓ/mg), comp is the fraction of the gas in the atmosphere (0.2095 for oxygen and 0.7808 for nitrogen), P_{atm} is the barometric pressure (atm.), and K_p is the conversion constant from atmospheres to depth of water (≈33.9 ft. H_2O/atm or 10.34 m H_2O/atm), assuming hydrostatic pressure.

Impact of Assuming a Zero Saturation Concentration for Methane

Eq. 7 assumes the saturation concentration of methane is small since the concentration of methane in the atmosphere is essentially zero. However, the concentration of methane in a bubble may not approximate zero due to methane transferring into the bubble from the water as the bubble is dragged through the plunge pool. Assuming all methane transfer occurs across a bubble interface, a mass balance of methane across the hydraulic structure is written as:

$$C_m=\frac{q_w}{q_a}(C_u-C_d) \quad (14)$$

where C_m is the concentration of methane in a bubble as it is released to the atmosphere, C_u is the concentration of methane in the water upstream of the structure, C_d is the concentration of methane in the water downstream of the structure, q_w is the unit discharge of water (m^2/s), and q_a is the unit entrainment of air (m^2/s).

Measurements taken at the Rum River gated OG spillway were used to assess the impact of assuming a methane saturation concentration of zero. C_u and C_d were measured at 16.58 and 8.72 mg/m^3(ppb), respectively. q_w was calculated from the gate opening, head, and geometry of the structure to be 0.167 m^2/sec. The specific discharge of the entrained air was measured directly using a 1m x 1m square hood designed and built by Steven C. Wilhelms. The hood was placed on the water surface in the plunge pool capturing the air released to the atmosphere by the bubbles. The hood constricted into a 2 cm diameter pipe, where a hot film anemometer was placed to measure velocity, enabling the air discharge coming out of the water to be calculated. These measurements are given in the Appendix. The hood was moved laterally and longitudinally along the tailrace in the region where air bubbles were escaping and the air flow rates were summed to yield the total air discharge. The specific air discharge was then calculated. For this experiment q_a was computed from these measurements to be 0.125 m^2/sec.

Then, using Eq. 14 to compute the released concentration

of methane for a bubble:

$$C_m = \frac{0.167\,(m^2/s)}{0.125\,(m^2/s)}\,(16.58-8.72)\,mg/m^3 = 10.5\,mg/m^3 \qquad (15)$$

The equilibrium concentration of methane, C_{me}, in a bubble downstream of the structure can be found from the Henry's Law relationship:

$$C_{me} = C_d \cdot H_{CH_4} \qquad (16)$$

where H_{CH4} = dimensionless Henry's Law constant for methane = 17.98 at 0°C. Using Eq. 16 to calculate C_{me}:

$$C_{me} = 8.72\ mg/m^3\ (17.98) = 156.8\ mg/m^3 \qquad (17)$$

Therefore, the concentration of methane in a bubble as it is released to the atmosphere is 6.7% of the equilibrium concentration of methane in that bubble.

The transfer efficiency of methane can be calculated by rewriting Eq. 6 in terms of Henry's Law constant:

$$E_m = \frac{C_d - C_u}{\left(\frac{C_b}{H_{CH_4}}\right) - C_u} \qquad (18)$$

where C_b is an average value of the methane concentration in the bubble, or:

$$C_b = \left(\frac{1}{2}\ C_m\right)\left(1 + \frac{D_{eff}}{10.3}\right) \qquad (19)$$

The concentration of methane in the bubble varies as the bubble is washed through the plunge pool. At the inception of the bubble, the concentration is approximately zero, since there is relatively little methane in the atmosphere. As the bubble is released to the atmosphere at the end of the plunge pool, the concentration is C_m. The first term in Eq. 19 is an arithmetic mean of the endpoint concentrations. The second term of Eq. 19 accounts for the increase in concentration due to the reduction in volume of a discrete bubble as it is dragged to some depth in the plunge pool. For the example used herein, D_{eff} was computed from a comparison of oxygen and methane transfer measurements to be 0.8 m.

Solving Eqs. 18 and 19:

$$C_b = \frac{1}{2}\ (10.5)\left(1 + \frac{0.832}{10.3}\right) = 5.7\ mg/m^3 \qquad (20)$$

$$E_m = \frac{8.72-16.58}{\left(\frac{5.7}{17.98}\right) - 16.58} = 0.48 \qquad (21)$$

When the concentration of methane in a bubble is ignored, $C_s=0$ and Eq. 7 becomes:

$$E_m = \frac{8.72-16.58}{-16.58} = 0.47 \qquad (22)$$

Thus, the difference in transfer efficiencies calculated by accounting for a concentration of methane in the bubble and by ignoring the concentration of methane in the bubble is only 1.9% of the transfer efficiency. This is well within the uncertainty of the measurements and was incorporated as a bias uncertainty in the calculations.

Further calculations using a predictive relationship for the q_a (Ervine and Elsawy, 1975) calibrated to these measurements for entrained air discharge indicated that the bias of roughly 2% would apply to all discharges at this structure.

IV. SAMPLING TECHNIQUE

Oxygen and methane measurements were taken at all of the structures tested. Additionally, total dissolved gas measurements were taken at the Rum River structure to determine dissolved nitrogen concentration. At each site, as upstream sampling location was chosen as close to the structure as possible to assure that the water sampled was representative of the water passing over the structure. The downstream sampling point was chosen close to the structure, yet downstream of the air entrained or bubbly region of the plunge pool. At both upstream and downstream sampling points, measurements were taken near the water surface, at mid-depth, and near the bottom to check for stratification of methane or oxygen.

Dissolved Oxygen Sampling

Dissolved oxygen measurements were performed in-situ with a YSI No. 58 dissolved oxygen probe and meter. The probe was lowered to the appropriate sampling depth along a weighted tether to the probe from drifting to the surface in locations of high stream velocity. The meter reading of either concentration (mg/ℓ) or percent of saturation was recorded. The saturation concentration, C_s was determined as:

$$C_s = \frac{.0295\ P_{atm}}{H} \qquad (23)$$

where H is Henry's Law and P_{atm} is atmospheric pressure. Gulliver and Rindels (1986) found the actual saturation concentration in river water to be 98±2% of the values listed in the literature.

Total Dissolved Gas Sampling

The total dissolved gas concentration was measured in situ at the Rum River structure using a modified 'gasometer' (Bouck, 1982) consisting of a gas permeable tubing connected to a pressure transducer as shown in Photo. 1. The gasometer was also lowered to the appropriate depth along the weighted tether. After allowing the gasometer to equilibrate, the voltmeter reading from the pressure transducer was recorded. In most cases it took approximately 15 to 20 minutes for the gasometer to equilibrate. The transducer was calibrated before each field trip to yield a known pressure for a given signal, as shown in Fig. 5. The scatter of the calibration points shown in Fig. 5 is within the range of uncertainty reported by the manufacturer. The slope of the calibration was determined from linear regression and the uncertainties reported by the manufacturer were included in the uncertainty of our measurements.

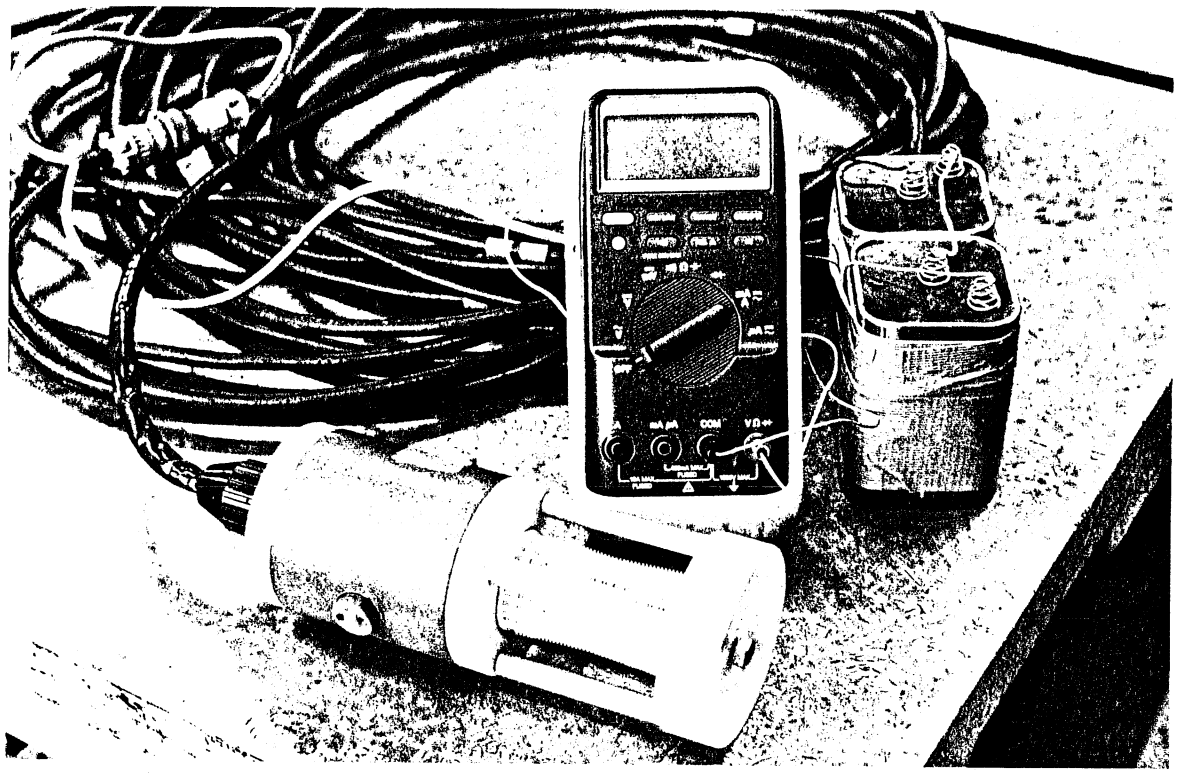

Photo 1 - Total dissolved gas meter

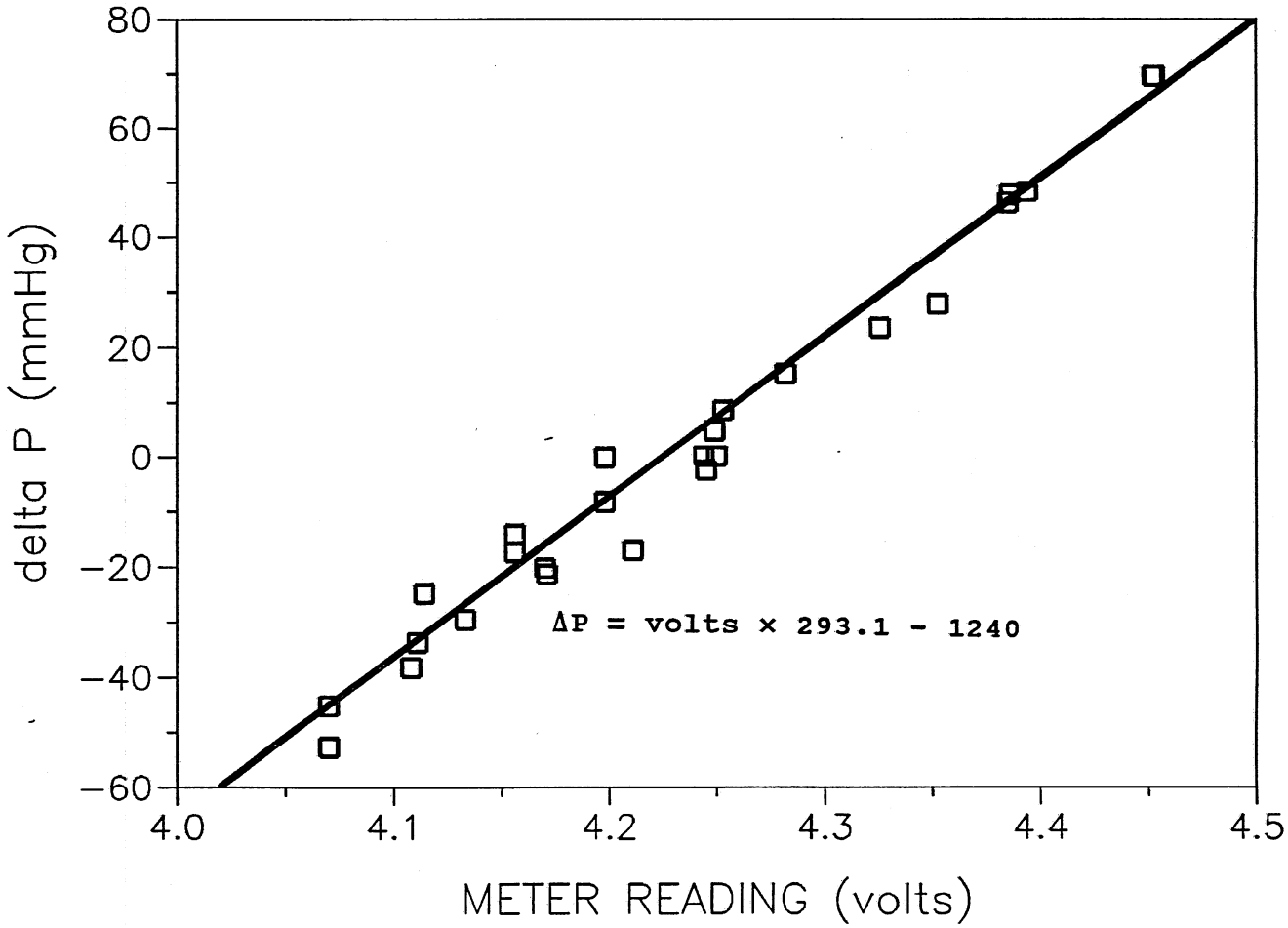

Figure 5 - Total gas meter calibration

The dissolved nitrogen concentration, C_{N2}, was computed as:

$$C_{N_2} = \frac{P_{N_2}}{H_{N_2}} \quad (24)$$

where H_{N2} is the Henry's Law constant for nitrogen and P_{N2} is the partial pressure of nitrogen inside the tubing calculated as:

$$P_{N_2} = 98.77\% \ (P - P_{O_2} - P_{H_2O}) \quad (25)$$

where P is the total dissolved gas pressure (measured with the gasometer), P_{H2O} is the vapor pressure of water, and P_{O2} is the partial pressure of oxygen in the tubing calculated as:

$$P_{O_2} = O_2\% \ (P_{atm} - P_{H_2O}) \ O_2 \text{mole fraction in dry air} \quad (26)$$

where $O_2\%$ is the percent saturation of oxygen in the water, P_{atm} is the barometric pressure, and P_{H2O} is the vapor pressure of water. The mole fraction of oxygen in dry air is 0.2095 (Weast, 1976).

Methane Sampling

Methane sampling was performed by collecting water samples in the field and later analyzing those samples in the laboratory using the headspace analysis technique (described in Section VI). Water samples were collected in 40 mℓ borosilicate glass vials with teflon faced septa and open top screw caps. The uncapped empty vials were loaded in the sampling device shown in Photo. 2. The sampler was rapidly lowered to the appropriate depth. Water enters the sampler through the side tubings and air exits the sampler through the top tube. This design virtually eliminates bubbling within the sampler that could result in stripping of methane from the water. Once filled, the sampler was removed from the water. The vials were capped, teflon side down, under water while still in the sampler in order to reduce the volatilization of methane to the atmosphere. The capped samples were packed top down to prevent the loss of methane due to bubble formation caused by temperature change and subsequent leakage through the septa or cap.

Sample Preservation

As samples were not analyzed immediately after they were gathered, some method of preservation had to be employed. Schultz et al. (1971) concluded that 1 mℓ of 37% formalin solution in a 60 mℓ solution preserved the sample for seven days. To stop bacterial action other researchers have raised

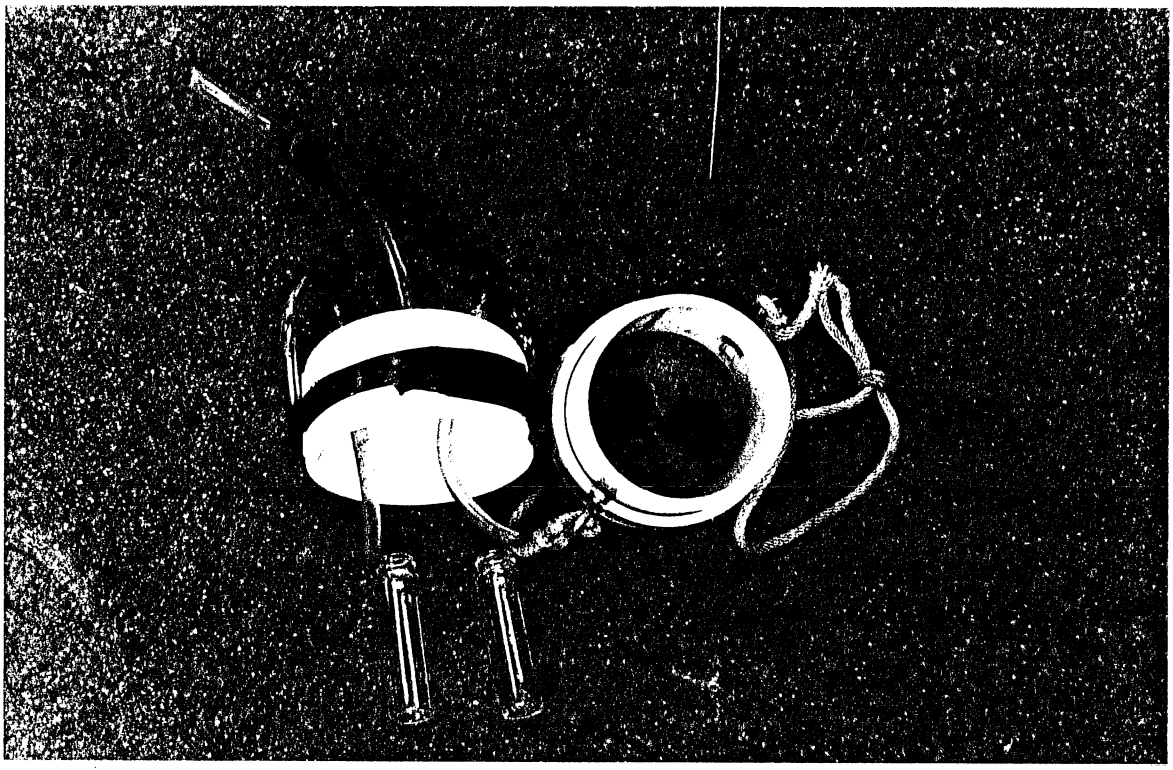

Photo 2 - Water sampler

the pH to 11, added HgCl or stored samples on ice. It was decided to test 0.5 mℓ and 0.25 mℓ of 37% formalin solution to preserve the samples. Samples were gathered from the Anoka Dam on the Rum River and from the Mississippi River in Minneapolis. As can be seen from Fig. 6, the methane concentrations with 1/4 mℓ formalin and with no formalin decreased with time. The samples with 1/2 mℓ formalin were relatively constant. Therefore, it was decided to use 1/2 mℓ of formalin as a preservative for this study. The formalin was injected in the samples as soon as possible after collection and before transport.

Sample Transporting

The samples were transported to the gas chromatograph (GC) laboratory at the University of Minnesota, Department of Civil and Mineral Engineering for analysis. Samples obtained near the University were transported immediately by car, whereas samples obtained elsewhere were shipped via overnight express couriers.

All water samples collected at a given location exhibited a certain degree of precision uncertainty in methane concentration. However, those samples shipped by overnight couriers exhibited such a large precision uncertainty in methane concentration that for all practical purposes the samples were useless. Tables 1 and 2 show that sample vials collected at the same location and time, and even from the side by side bottles in the same sampler grab, varied in methane concentrations by as much as 69%. While there is a possibility that this is truly representative of the actual concentrations, it is extremely unlikely that there is that much of a variation in methane concentrations due to the turbulent mixing at structures. A more likely explanation for the large variances in concentrations is that there was a depletion of methane from some of the sample vials during shipping.

Although the samples were packed upside down, there is no way of knowing if the samples remained upside down for their entire journey to Minneapolis. Perhaps bubbles of high methane concentration formed and leaked out the bottle-septa seal, or though a piercing hole in the septa while inverted. The potential for methane loss during transport is increased by the atmospheric pressure drop exerted on the samples during airplane transport. Fig. 7 shows possible methane evasions routes. In light of the methane concentration randomness of the samples transported by air freight, an alternative method of transport is clearly needed.

Alternative Sample Shipping Technique

An alternative packing and shipping technique has been developed and is currently being tested. The technique is

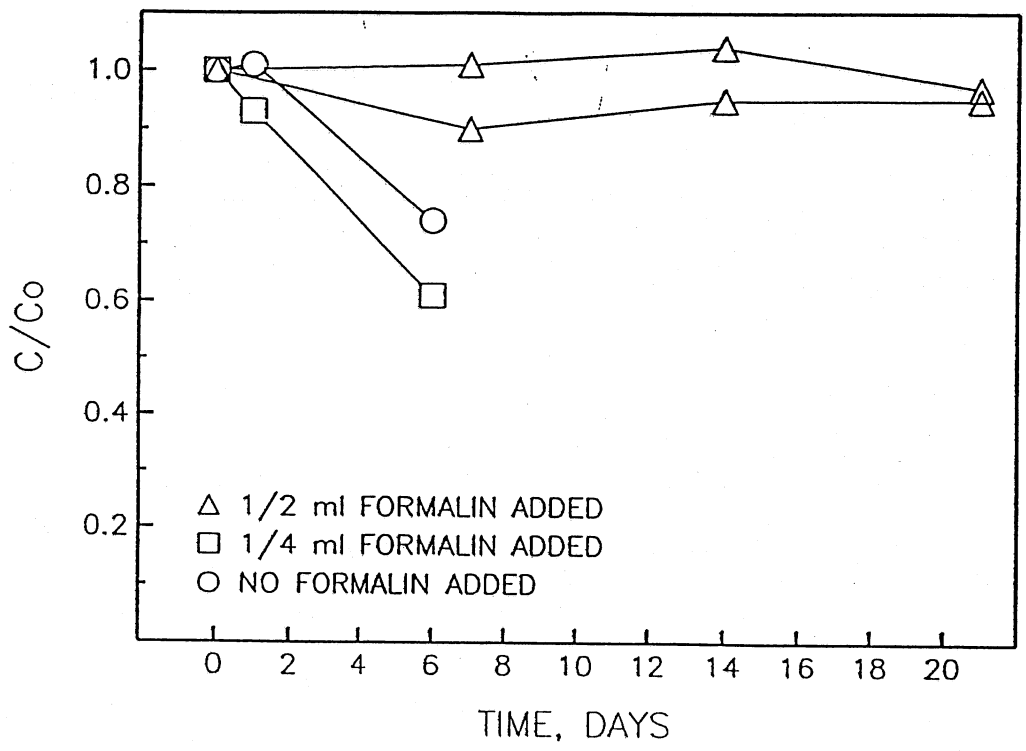

Figure 6 - Effect of formalin on methane concentration

Table 1 - Methane Concentrations; Opekiska Lock and Dam, Sept. 24, 1992.

Location	Gate Opening (ft.)	Sample Depth (ft.)	Time of Sampling	Bottle #	$[CH_4]$[1] ($\mu g/\ell$)
upstream	0.3	15	8:30	32	8.22 ± 0.44
				31	8.43 ± 1.36
				23	7.78 ± 0.33
				24	8.61 ± 3.32
	0.3	10	15:12	71	11.39 ± 3.17
				72	14.08 ± 2.92
				46	9.73 ± 0.52
downstream	0.1	5	9:20	43	5.65 ± 0.09
				45	5.18 ± 0.28
				15	5.30 ± 0.41
				38	6.17 ± 0.12
	0.3	5	9:00	17	6.14 ± 0.05
				35	5.69 ± 0.34
				29	5.55 ± 0.14
				33	5.29 ± 0.03
	0.5	5	9:35	36	5.38 ± 0.18
				58	6.39 ± 0.49
				42	5.40 ± 0.42
				50	4.98 ± 0.05
	0.75	5	13:30	39	5.10 ± 0.48
				40	4.37 ± 0.14
	1.0	5	13:40	48	4.17 ± 0.07
				47	5.17 ± 0.53
				56	4.33 ± 0.20
				64	4.59 ± 0.17
	1.5	5	13:55	54	5.14 ± 0.83
				55	4.22 ± 0.25
				70	3.95 ± 0.06
				62	4.57 ± 0.19
	2.0	5	14:10	60	4.67 ± 0.13
				68	5.30 ± 0.48
				63	5.37 ± 0.15
				61	5.51 ± 1.34

[1]Uncertainties include only precision uncertainty.

Table 2 - Methane Concentrations; Smithland Lock and Dam, Sept. 23, 1992.

Location	Gate Opening (ft.)	Sample Depth (ft.)	Time of Sampling	Bottle #	$[CH_4]$[1] ($\mu g/\ell$)
upstream	2.0	15	11:57	30	3.08 ± 0.09
				22	2.89 ± 0.19
				41	3.58 ± 0.29
				49	2.75 ± 0.14
downstream	0.5	15	9:40	9	10.22 ± 0.54
				10	7.66 ± 0.55
				12	12.16 ± 0.49
	1.0	15	10:05	6	7.17 ± 0.08
				14	6.63 ± 0.75
				7	6.95 ± 0.20
				16	7.33 ± 1.32
	1.5	15	10:25	13	5.55 ± 0.59
				25	6.06 ± 0.87
				5	6.71 ± 0.47
	2.0	15	10:55	20	6.74 ± 0.56
				21	6.58 ± 0.56
			11:00	35	5.14 ± 0.28
				28	5.44 ± 0.30

[1]Uncertainties include only precision uncertainty.

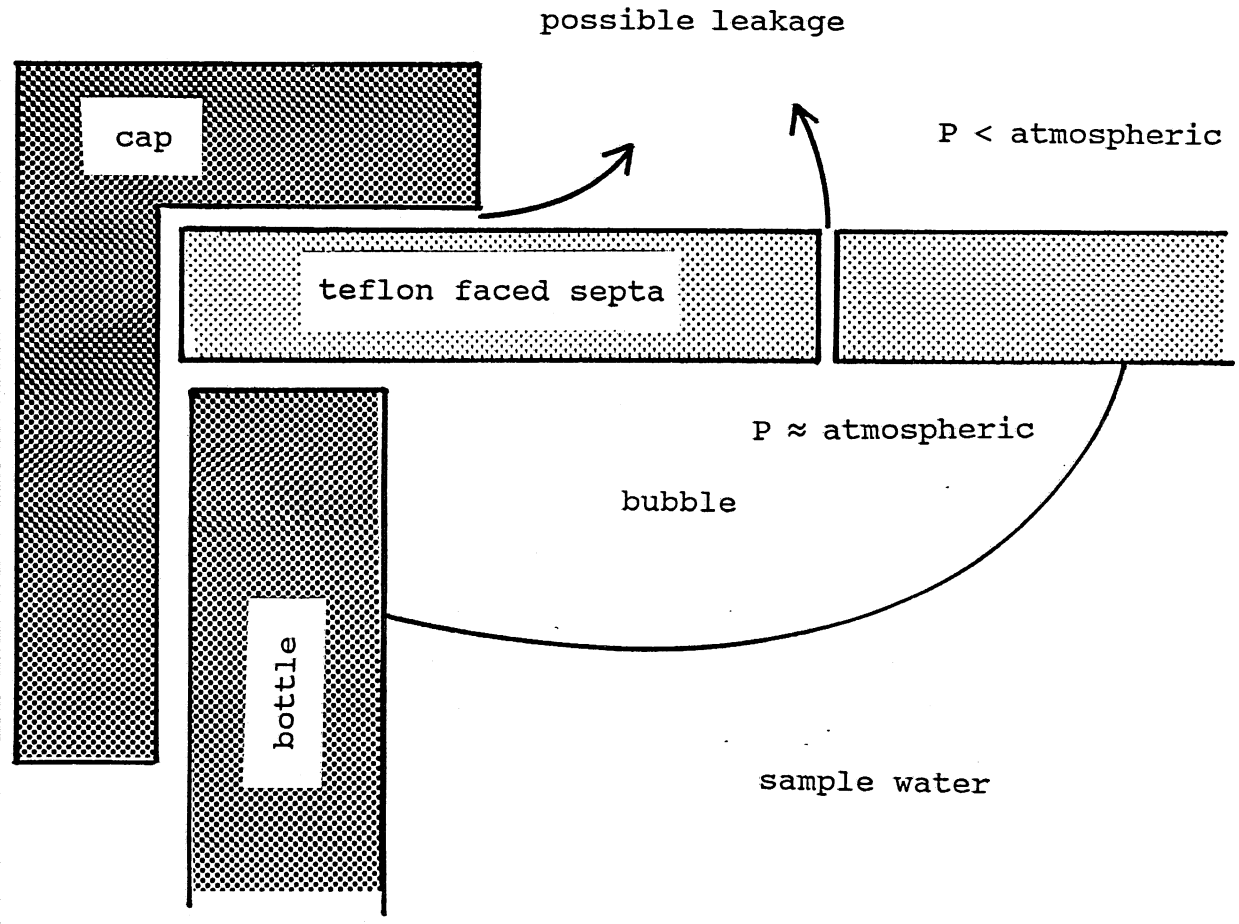

Figure 7 - Potential evasion routes of methane during sample transport

referred to as the 'double redundancy technique.' The basis of the technique is that the sample vials are packed upside down immersed in a water bath. The technique is doublely redundant since first, the risk of the of the inverted sample being righted is reduced. The package handlers will be less likely to tip over a package labeled "↑ LIQUID- THIS END UP ↑" in order to avoid a spill (actually, a spill would be very unlikely due to the watertight packaging). Secondly, even if the sample vials are righted, there is less potential for methane escape due to the vials being packed in a water bath. Fig. 8 shows the restricted flow through a potential leak in a septa. The surface tension of the water on the outside face of a septa will prohibit the flow of gas from an air bubble on the bottle side of a septa.

In practice, an empty one-gallon paint can could be used as the container. The vials could be cushioned with sponge or foam packing. The packing would also serve as a spacer to keep the septa of all vials below the water surface inside the can, regardless of the upward orientation of the can. No results on the effectiveness of the technique are available as of this writing since the technique is currently being tested.

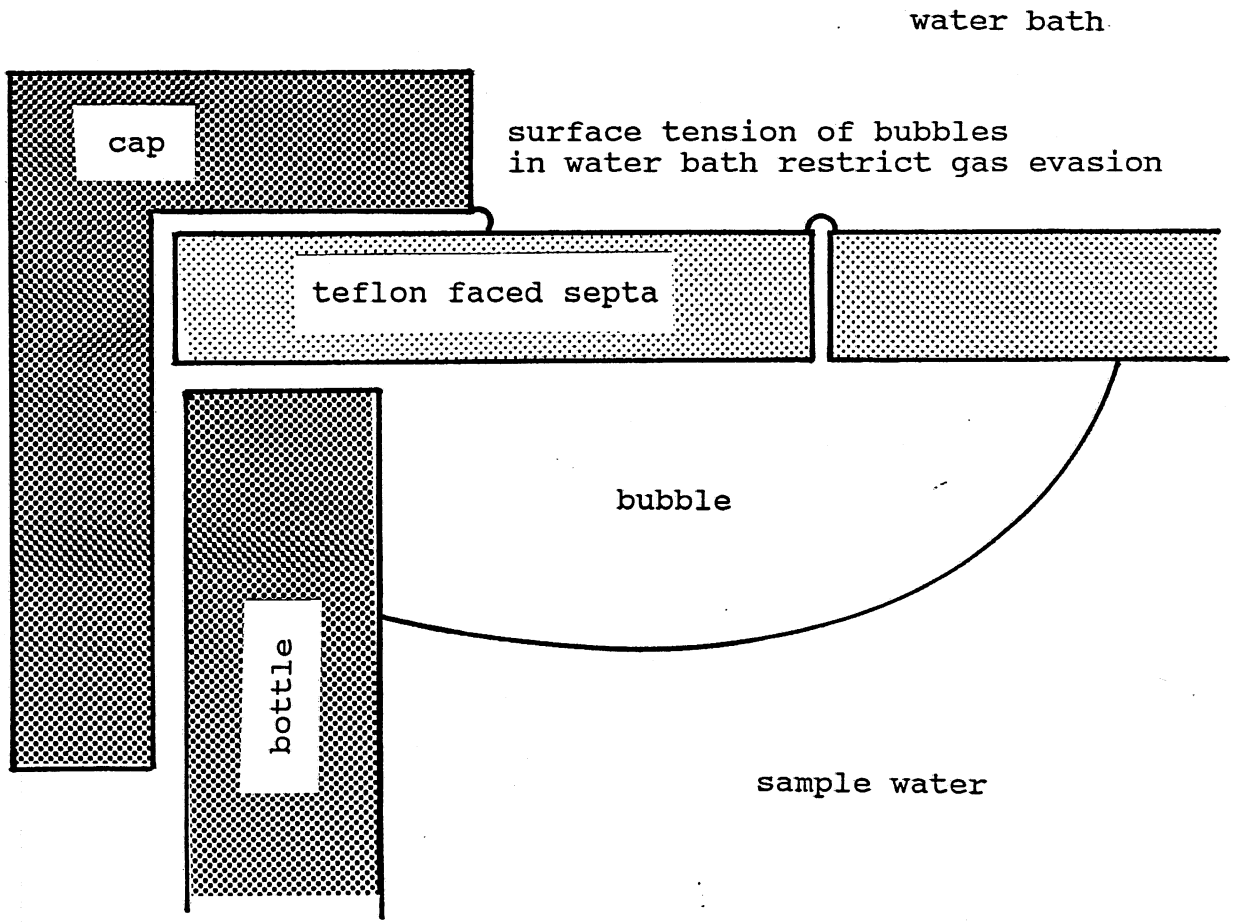

Figure 8 - Restricted flow of gas from sample immersed in water bath

V. HEADSPACE ANALYSIS TECHNIQUE

A slightly modified version of the headspace analysis technique developed by Thene and Gulliver (1990) was used to determine the concentration of methane in the water samples by measuring the methane concentration of the air in equilibrium with the water.

Calculation of Methane Concentration in Water

The concentration in the headspace, C_a, is given by Thene and Gulliver (1990) as:

$$C_a = C\left[\frac{RT}{MH} + \frac{V_a}{V_w}\right]^{-1} \qquad (27)$$

where C is the concentration in the water prior to the creation of the headspace, R is the universal gas constant, T is the water temperature, M is the molar mass of methane, H is the Henry's Law constant for methane, V_a is the volume of the headspace in the sample bottle, and V_w is the volume of the water in the sample bottle. The exact volumes of headspace and water in the samples used in Eq. 27 were determined by weighing each bottle before creating the headspace, after creating the headspace, and when empty.

Creating the Headspace

A headspace was created in each sample vial at the GC laboratory. Photo. 3 shows the method used to make the headspaces. A drainage needle open to the atmosphere was inserted in the septa of the upside down vial. Approximately 10 mℓ of nitrogen gas were injected through the septa at the top of the vial, forcing water out through the drainage needle. Samples were then shaken vigorously for 60 seconds to strip the methane from the water into the headspace.

Gas Chromatography

The gas chromatograph (GC) used was a Hewlett Packard 5890A equipped with a flame ionization detector (FID), a strip chart recorder and an electronic integrator and a 4 ft. long 5A 60/80 molecular sieve.

Five separate 200 μℓ volumes were withdrawn from the headspace of each bottle with a 250 μℓ gas tight syringe and then injected into the GC. At least three injections were needed to accurately compute the precision uncertainty of the measurement; five was chosen as a matter of convenience. The pressure in the headspace was kept nearly constant by counter-injecting 200 μℓ of water into the sample prior to withdrawal of the GC injection.

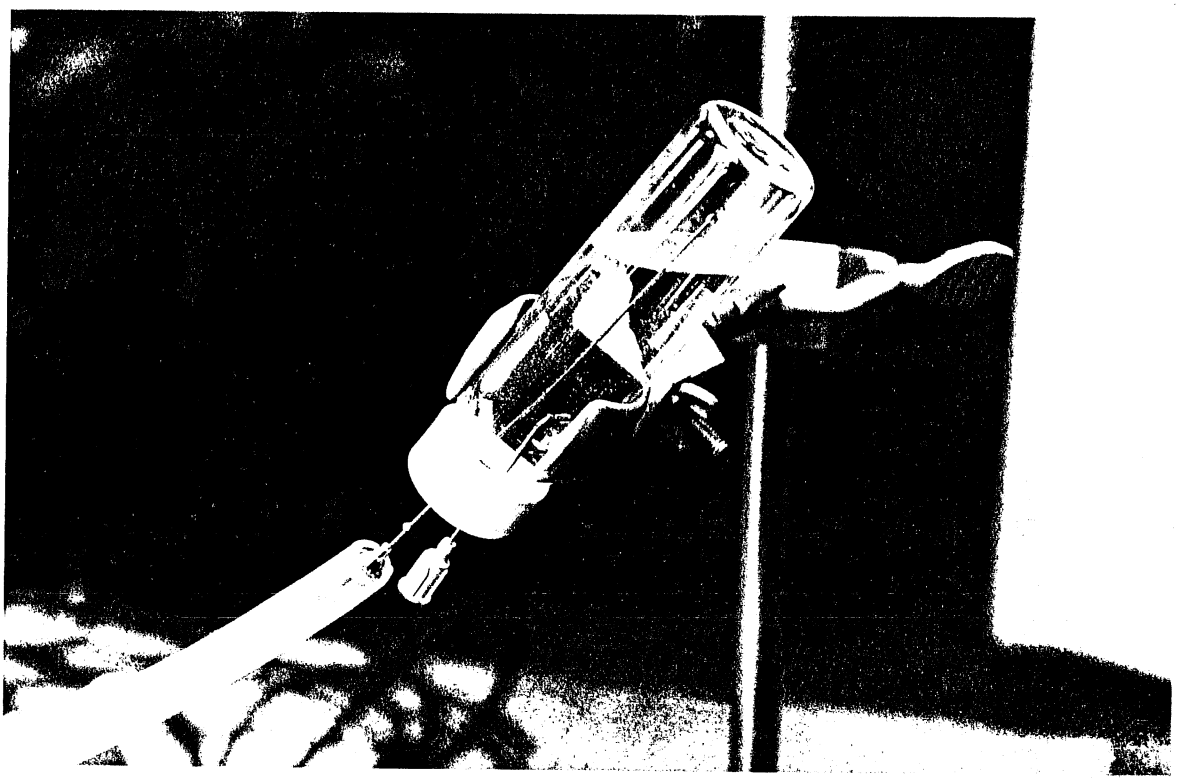

Photo 3 - Creation of headspace in sample bottle

The water used to replace the sample volume must not contain methane. Headspace analysis of de-ionized water, tap water, and Mega-Pure water showed that only the Mega-Pure water sample did not give a GC response. Therefore, only Mega-Pure water was used to replace the extracted 200 $\mu\ell$ volumes. The injection of 1 mℓ of Mega-Pure water does slightly affect the methane concentration of the headspace. However, the effect is small due to methane's high volatility (McDonald and Gulliver, 1992 and Thene and Gulliver, 1990).

Calibration of the GC was performed by injecting different volumes of 100 ppm (by volume) methane standard and plotting the results. A curve was then fit through the calibration points to obtain an equation relating area count to mass of methane, as shown in Fig. 9. This mass was then related to concentration in the original sample as described in McDonald and Gulliver (1992). Uncertainties in the concentration measurements were also computed to the 95% confidence interval. The confidence interval was typically ± 1 to 2 percent of the measured concentration.

A quality control/quality assurance program was also carried out to assure that the concentrations in the water column were, within the confidence limits, correctly determined from the GC readings. Tests were performed on the length of time the samples could be preserved, the quantity of formalin required for preservation, the technique of sample injection into the GC, the impact of headspace pressure change due to sampling, the GC response of formalin, the reuse of septa, and the effect of bubble formation in the vials (McDonald and Gulliver, 1992).

Injection Technique

It was discovered that the speed in which the sample was injected into the GC led to different responses. To test the effects of injection speed, different volumes of standard were injected into the GC at different speeds. Three speeds were tested. The first speed was to inject as fast as possible. The total time to pierce the septa, depress the plunger, and withdraw the syringe was under 0.5 seconds. The second speed was a three second process. One second was used to pierce the septa and to get the syringe in place. Two seconds were used to depress the plunger than then the syringe was withdrawn quickly. The third speed tested was similar to the second only four seconds total were required for the entire injection process. As shown in Fig. 10, the fast injection yields a different response from the other injection speeds. Thus, if the injection speed is 0.6 seconds instead of 0.5 seconds, the results could be different. The other two plots are virtually identical, indicating that the results were very nearly insensitive to injection speed for the three- and four-second injection. Therefore, it was decided to use the three-second injection for samples. It is thought with the fast injection

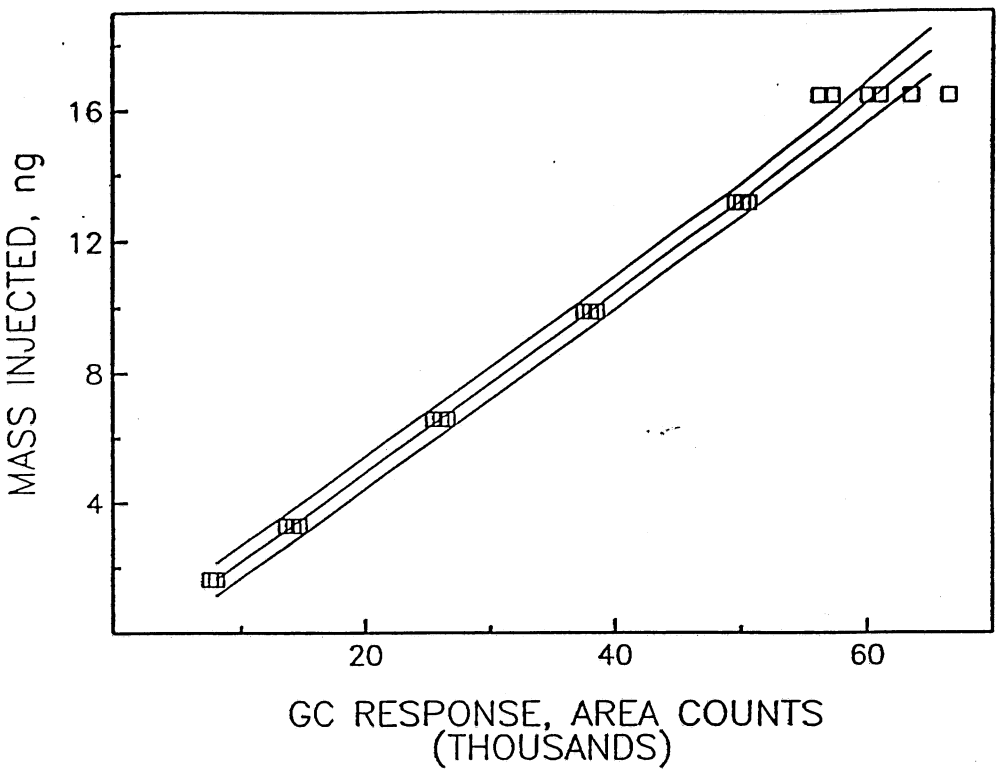

Figure 9 - GC Calibration

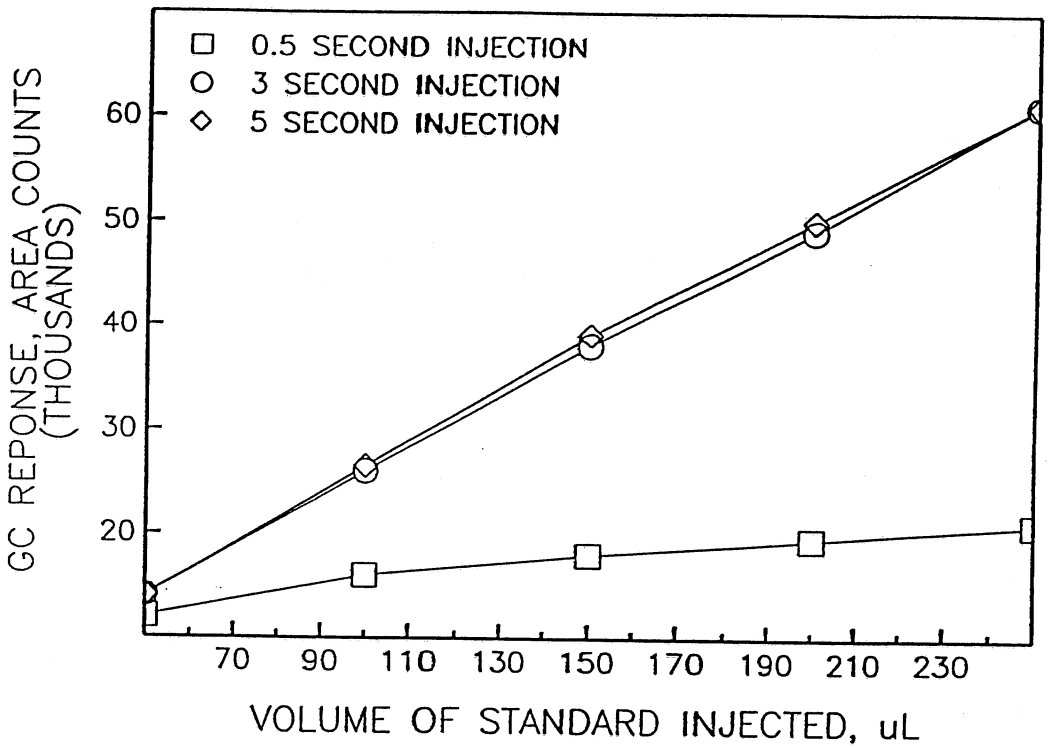

Figure 10 - Impact of injection speed on GC response

that some of the sample is lost through the pierced septa in the injection port of the GC or through the plunger seal in the gas tight syringe.

Limit of Detection/Limit of Quantification

The limit of detection, LOD, is defined as the lowest concentration that is statistically different than the blank. The limit of quantification, LOQ, is the concentration level above which quantitative results can be obtained with confidence. In most cases the LOD and LOQ are defined as three and ten times the standard deviation of the response to blank runs, respectively (American Chemical Society, 1983). Experience has shown that there is no "methane" response to blank runs. Consequently, a different procedure was required. It was decided that an appropriate LOD and LOQ could be determined by injecting various masses of the standard gas each 10 times into the GC and calculating the standard deviation of each sub-set of injections. Then the LOQ was defined as the point where ten times the standard deviation of a set of injections equaled the average area count of the set of injections. Or LOQ = C when $C = 10\sigma$, where C is the mean concentration and σ the standard deviation in concentration measurements. Similarly the LOD was defined as the point where three times the standard deviation equaled the average area count.

Using this definition and the information gathered from the injection of standard gas, Table 3 was prepared. This table shows the LOQ to lie between the mass contained in 3 and 5 $\mu\ell$ of standard gas. By linear interpolation between these two points the mass of LOQ was equal to 0.000211 μg. Assuming a 250 $\mu\ell$ sample injection, the headspace concentration would be:

$$C_a = \frac{mass}{volume} = \frac{0.0002112\mu g}{250\mu\ell} = 0.84\mu g/\ell \qquad \textbf{(28)}$$

Since the volume of headspace is roughly 10 mℓ and the volume of water is roughly 30 mℓ, the pre-headspace water concentration is computed from Eq. 12 as:

$$C = (0.04+0.33)\,C_a = 0.37\,C_a = 0.3\mu g/\ell \qquad \textbf{(29)}$$

This is the value for LOQ. LOD is defined as 3/10 of the LOQ such that:

$$LOD = \frac{3}{10}\,LOQ = 0.1\mu g/\ell \qquad \textbf{(30)}$$

Table 3 - Data Used for LOQ Analysis

Volume (μℓ)	Mass (μg)	Mean AC	10 σ	10σ/mean	Equivalent Water Concentration (μg/ℓ)
150	0.009963	35045.1	5539.3	0.16	14.7
100	0.006642	22996.1	7456.6	0.32	9.5
50	0.003321	12192.9	4356.6	0.36	4.9
10	0.000664	2886.8	1658.2	0.57	0.98
5	0.000332	1891.4	1118.3	0.59	0.49
3	0.000199	1007.1	1047.5	1.04	0.29

Bubble Formation

Bubbles may be formed in the samples as the samples are transported from cold temperatures to warmer temperatures. A calculation was thus made to determine if the bubbles formed would significantly affect the methane concentration in the sample. For this calculation, a 3 mm diameter bubble and a water methane concentration of C = 20 $\mu g/\ell$ were assumed. Eq. 27 then becomes:

$$C_a = 20\mu g/\ell \ (0.037+0.00036) = 535 \ \mu g/\ell \qquad (31)$$

The percentage of the total methane in the sample bottle that is in the bubble, $\%CH_{4\ bubble}$, is:

$$\%CH_{4\ bubble}=100\frac{C_a V_a}{C V_w}=0.96\% \qquad (32)$$

The bubble would remain in the vial upon headspace injection and would become a part of the headspace. If 10 ml of water is removed, while 30 ml remain, the headspace concentration for this example would be high by 1/4(0.96%) = 0.24%. This percent difference is insignificant compared to the precision of the GC analytic technique for methane.

VI. RESULTS

The results of simultaneous methane-oxygen transfer at four structures are summarized in Table 4. Descriptions of the structures are included in the Appendix. Fig. 11 shows the effective depth plotted versus specific discharge at Rum River for six separate field trips. Fig. 12 is a similar plot for the St. Cloud structure on 3/15/90 and 4/5/93. The calculated effective depth at the Anoka structure is reproducible as a function of specific flow rates for a variety of water temperatures, upstream oxygen deficits, and heads. The effective depths at the St. Cloud differ from those at the Rum River structure for comparable specific discharges, perhaps due to differences in head, tailwater depth, and plunge pool design.

Generally, as the specific discharge increases, the effective depth increases. At low discharges, the momentum of the plunging jet is insufficient to carry the bubbles deep into the pool, and the effective saturation concentration is close to local atmospheric concentration. At high discharges, the momentum of the plunging jet carries the entrained bubbles deeper into the pool, and the effective saturation concentration is significantly higher than that computed from local atmospheric concentration because of the higher pressures that the bubbles experience. Negative values of effective depth are listed in Table 4 for the lower discharges at the Kost and St. Cloud structures. There is no physical explanation for this. The actual effective depth values are most likely positive and the measurements are in error. In each case where a negative effective depth is calculated, there is a greater uncertainty in the reported effective depth. Thus, these negative values are small relative to the measurement uncertainty.

As a verification of the principles presented herein, effective depths were calculated from dissolved nitrogen measurements and from dissolved oxygen for a range of discharges, using methane as the tracer gas for both. Nitrogen and oxygen are both present in quantity in the atmosphere and therefore in the entrained bubbles. As a bubble is pulled to some depth in the plunge pool, the same hydrostatic forces increase the partial pressures of both oxygen and nitrogen proportionally to their atmospheric concentrations. This proportionally uniform increase in partial pressures leads to a proportionally uniform increase in the effective saturation concentrations, and ultimately a uniform increase in the effective depth. Thus, the effective depth calculated using dissolved nitrogen measurements should equal the effective depth calculated using dissolved oxygen measurements.

Table 5 shows the results of simultaneous methane, oxygen, and nitrogen transfer at the Rum River structure on 8/31/93. At each specific discharge tested, the effective

Table 4 - Results of Simultaneous Methane and Oxygen Transfer Measurements at Various Hydraulic Structures. Uncertainty is given to the 95% confidence level.

Structure	q	Oxygen			Methane			D_{eff}	Tail-water Depth
		C_u	C_d	E	C_u	C_d	E		
	(m^2/s)	(mg/ℓ)	(mg/ℓ)		(μg/ℓ)	(μg/ℓ)		(m)	(m)
St. Cloud-Gated	0.16	10.05	11.84	.50±.05	7.95	4.20	.47±.04	-0.3±0.3	5.7
3/15/90	0.32	10.06	11.67	.45±.04	7.95	4.00	.50±.05	-0.6±0.3	5.7
T_{water}=0.0 °C	0.63	10.07	12.08	.56±.05	7.95	3.30	.58±.08	-0.4±0.3	5.8
O_2 C_s=13.63 mg/ℓ	1.27	10.09	12.45	.67±.06	7.66	4.14	.46±.08	0.6±0.6	5.8
P_{atm}= 724.05 mmHg	2.09	10.11	12.28	.62±.06	7.66	4.97	.35±.08	1.3±0.9	5.8
	2.93	10.13	10.67	.15±.06	7.66	7.35	.04±.08	6.0±16.6	5.8
	3.61	10.15	10.79	.18±.02	7.66	7.21	.06±.07	4.2±8.3	5.8
4/5/93	0.39	13.06	13.32	.31±.13	4.48	2.71	.40±.07	-0.4±0.3	5.7
T_{water}=0.9 °C	0.79	13.06	13.51	.52±.20	4.48	2.83	.37±.07	-0.1±0.3	5.8
O_2 C_s=13.92 mg/ℓ	1.18	13.06	14.09	1.19±.45	4.48	2.98	.33±.07	1.1±0.5	5.8
P_{atm}= 745.0 mmHg	1.58	13.06	14.35	1.50±.57	4.48	2.71	.40±.07	1.2±0.5	5.8
Rum River-Gated	0.16	8.05	11.97	.67±.04	15.20	6.13	.60±.04	1.0±0.5	3.2
3/2/90	0.35	8.05	11.69	.63±.03	15.20	7.63	.51±.03	1.1±0.5	3.3
T_{water}=0.1 °C	0.66	8.05	11.27	.55±.03	15.20	10.1	.33±.03	2.9±0.8	3.3
O_2 C_s=13.86 mg/ℓ	1.26	8.05	10.97	.50±.03	15.20	10.7	.29±.03	3.2±0.9	3.4
P_{atm}=738.4 mm Hg	1.81	8.05	10.65	.45±.03	15.20	11.7	.25±.02	3.4±0.8	3.5
	2.3	8.05	10.44	.41±.02	15.20	12.7	.21±.02	4.1±1.0	3.7
8/31/93	.78	6.89	8.89	1.05±.11	7.48	3.23	.57±.03	1.5±0.2	3.4
T_{water}=19.6 °C	1.10	7.06	8.89	1.05±.12	7.48	3.36	.55±.03	1.5±0.3	3.4
O_2 C_s=8.80 mg/ℓ	1.42	7.11	8.93	1.08±.13	7.48	3.42	.54±.03	1.6±0.3	3.4
P_{atm}=742.8 mm Hg	1.73	7.16	8.93	1.08±.13	7.48	3.78	.50±.03	1.9±0.3	3.7
	2.36	7.32	8.67	.91±.13	7.48	5.08	.32±.05	2.7±0.7	3.8
	3.15	7.36	8.56	.84±.12	7.48	4.99	.33±.03	2.1±0.5	3.8
6/22/93	0.97	8.04	9.48	2.06±.60	5.31	2.31	.56±.21	1.9±1.0	3.6
T_{water}=19.9 °C	1.21	8.04	9.50	2.09±.61	5.31	2.56	.52±.15	2.2±0.8	3.7
O_2 C_s=8.74 mg/ℓ	1.82	8.04	9.55	2.16±.63	5.31	3.09	.42±.20	3.0±1.7	3.8
P_{atm}=742.8 mmHg									

Table 4 (cont.)

Structure	q (m^2/s)	Oxygen C_u (mg/ℓ)	Oxygen C_d (mg/ℓ)	Oxygen E	Methane C_u (μg/ℓ)	Methane C_d (μg/ℓ)	Methane E	D_{eff} (m)	Tail-water Depth (m)
Rum River-Gated 2/17/90 T_{water}=0.1 °C O_2 C_s=13.86 mg/ℓ P_{atm}=744.3 mmHg	0.17	8.57	1.97	.64±.04	16.58	8.72	.47±.04	0.9±0.5	3.3
3/21/89 T_{water}=1.0 °C O_2 C_s=13.58 mg/ℓ P_{atm}=741.2 mmHg	0.16	7.41	11.58	.68±.03	16.25	8.10	.50±.07	1.1±0.8	3.4
3/25/93 T_{water}=0.1 °C O_2 C_s=14.02 mg/ℓ P_{atm}=746.5 mmHg	0.44	11.48	13.61	.84±.11	16.61	9.92	.40±.71	1.4±5.8	3.4
Rum River-Free Weir 3/2/90 T_{water}=0.1 °C O_2 C_s=13.86 mg/ℓ P_{atm}=738.4 mm Hg		8.05 11.63	11.63 12.00	.59±.03 .15±.03	15.13 7.66	7.66 7.30	.49±.04 .05±.04	0.4±0.8 3.2±8.7	0.6 0.6
Kost Dam-Free Weir 1/26/90 T_{water}= 0.4 °C C_s=13.73 mg/ℓ P_{atm}=739.6 mm Hg	0.05 0.05 0.05	8.57 8.58 9.34	10.59 10.53 11.01	.35±.02 .36±.02 .36±.03	54.01 48.48 53.55	33.30 34.49 37.45	.38±.07 .29±.02 .30±.06	-0.6±0.4 0.4±0.8 0.3±1.0	0.2 0.2 0.2

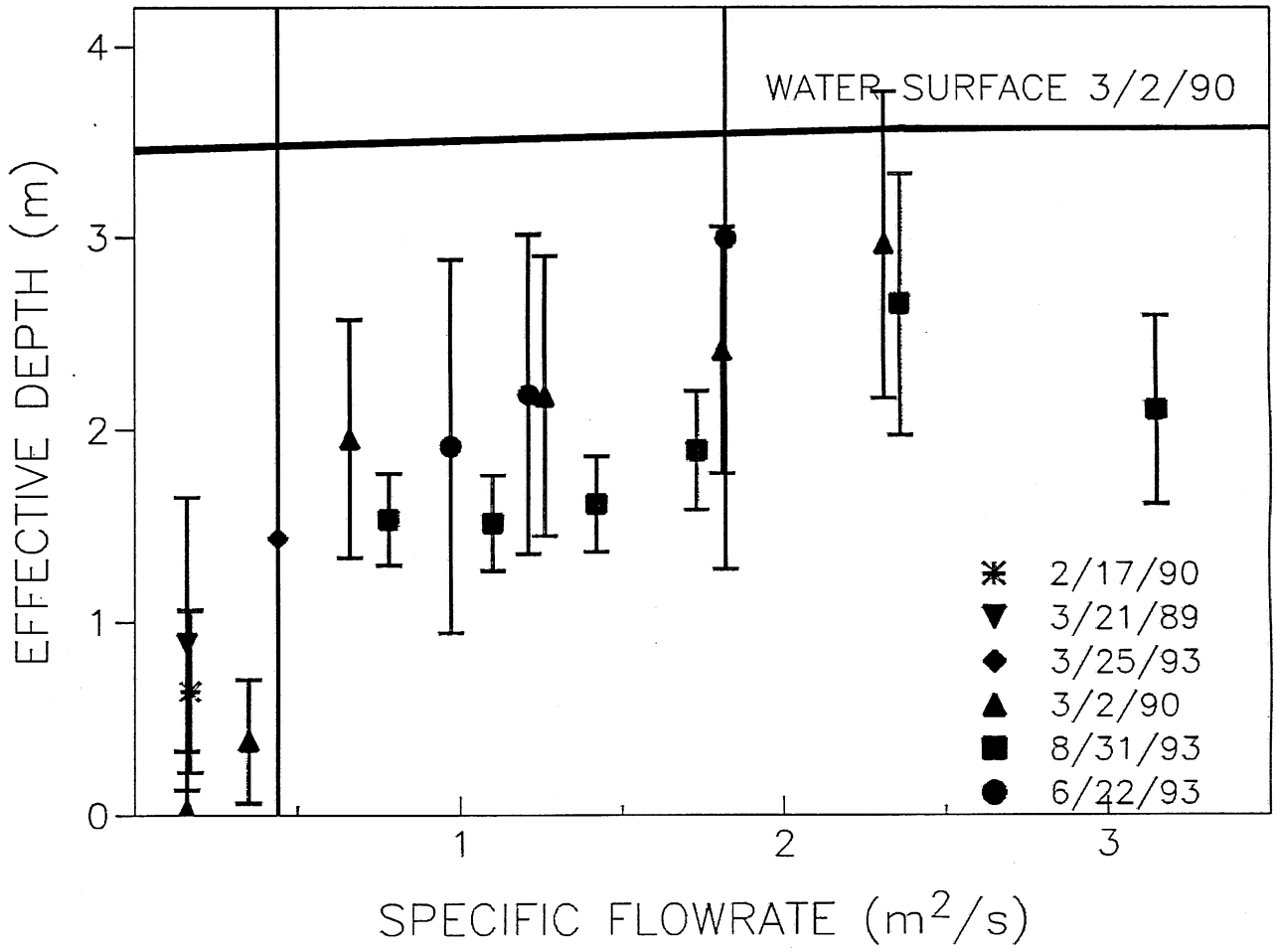

Figure 11 - Effective depth versus specific discharge at Rum River Dam

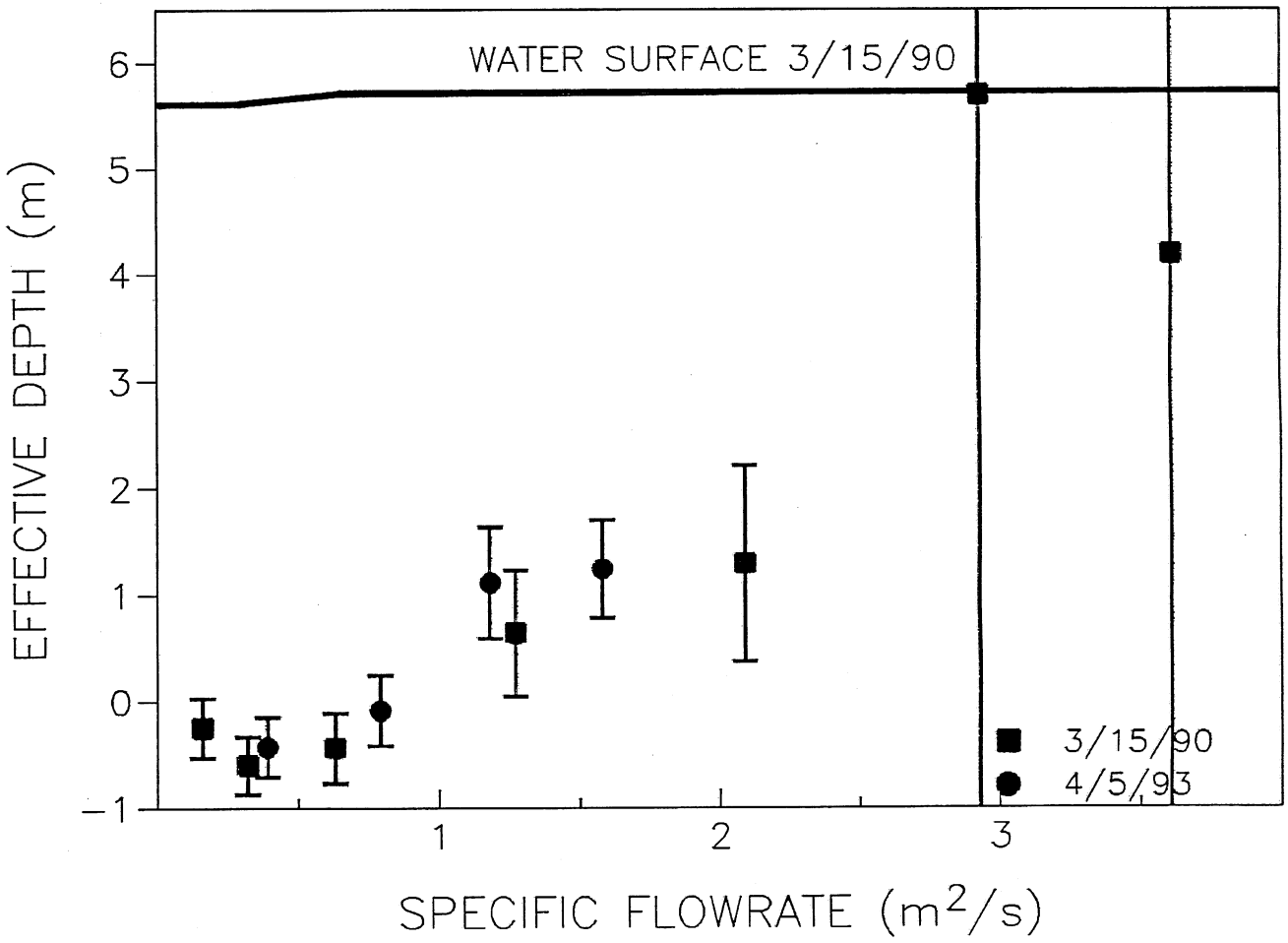

Figure 12 - Effective depth versus specific discharge at St. Cloud Dam

Table 5 - Results of Simultaneous Methane , Oxygen, and Nitrogen Transfer Measurements at Rum River Dam, 8/31/93.

Water Temperature = 19.6°C
Tailwater depth = 3.4 m
Barometric Pressure = 742.8 mmHg
O_2 Henry's Law constant = 17.78 mmHg·ℓ/mg
N_2 Henry's Law constant = 39.20 mmHg·ℓ/mg
O_2 saturation concentration = 8.74 mg/ℓ
N_2 saturation concentration = 14.72 mg/ℓ

	Methane			Oxygen				Nitrogen		
q (m^2/s)	C_u[1] (μg/ℓ)	C_d[2] (μg/ℓ)	E	C_u[3] (mg/ℓ)	C_d (mg/ℓ)	D_{eff}[2] (m)	C_u	C_d (mg/ℓ)	D_{eff}[2] (mg/ℓ)	(m)
.78	7.48	3.23±.05	.57±.03	6.89	8.89	1.53±0.24		14.72	16.42	1.78±0.39
1.10	7.48	3.36±.04	.55±.03	7.06	8.89	1.51±0.25		14.72	16.02	1.38±0.40
1.42	7.48	3.42±.01	.54±.03	7.11	8.93	1.61±0.25		14.72	16.09	1.49±0.40
1.73	7.48	3.78±.08	.50±.03	7.16	8.93	1.89±0.31		14.72	16.19	1.76±0.46
2.36	7.48	5.08±.23	.32±.05	7.32	8.67	2.65±0.68		14.72	16.24	2.82±0.83
3.15	7.48	4.99±.03	.33±.03	7.36	8.56	2.10±0.49		14.72	16.29	2.81±0.75

[1] Uncertainty in upstream methane concentration is 0.29 μg/ℓ.
[2] Uncertainties are given to the 95% confidence level.
[3] Assumes a linear increase in upstream DO over data collection period.

depth computed using dissolved nitrogen concentrations was found to be similar to the effective depth computed using dissolved oxygen data within the confidence interval of the measurement.

VII. CONCLUSIONS

1. Measurement of in-situ methane concentration is a viable technique for determining the transfer efficiency across a hydraulic structure or any device having a large rate of gas transfer and a relatively short residence time. It may also have other applications, such as measuring transfer efficiency in pneumatic diffusers.
2. Methane is usually not stratified in shallow reservoirs (less than 8 m deep) except under ice cover, where methane was found to be strongly stratified.
3. Because methane stratification in deeper reservoirs increases the uncertainty in determining the mean methane concentration at the top of the hydraulic structure, the methane tracer technique is most applicable to low head structures.
4. Oxygen and methane transfer efficiencies were found to be different when atmospheric pressure was used to compute oxygen saturation concentration and significant entrainment of air into the tailwater pool occurred. We believe that this difference occurs because entrained air bubbles pulled to a depth of higher pressure in the tailwater results in a larger saturation concentration for oxygen, while methane saturation is essentially zero throughout. This is a source of error in using the transfer efficiency of tracers to compute oxygen transfer efficiency and in using the measured oxygen transfer efficiencies to compute the transfer efficiencies of other compounds of interest, such the many volatile toxic compounds in our surface waters.
5. Simultaneous oxygen-methane transfer measurements and nitrogen-methane transfer measurements have been used to compute an effective saturation concentration that is a weighted mean of the saturation concentration that a submerged bubble experiences in its path through a hydraulic structure and plunge pool. The measurements have also been used to compute a similarly weighted mean depth of bubble penetration, called the effective depth, at two gated control structures.
6. Generally, as discharges increase, the effective depth increases, due perhaps to the increase momentum pulling the bubbles deeper in the plunge pool.
7. Measurements were used to compute the effective depth as a function of specific discharge on three different days at one structure. At comparable discharges, the effective depths were found to be similar within the confidence interval of the measurements.
8. The effective depth computed from oxygen-methane measurements was similar to that computed from nitrogen-methane measurements within the confidence interval of the measurements for a range of specific discharges at on structure, thus verifying the concept of effective depth.

9. More of these measurements need to be performed at other structures to relate the effective depth to parameters of the jet and structure. Only then can we make full use of our gas transfer measurements at hydraulic structures.

VIII. REFERENCES

Abram, Jeremy W. and David B. Nedwell, 1978. "Inhibition of methanogenesis by sulfate reducing bacteria competing for transferred hydrogen," Archives of Microbiology, 117, 89-92.

American Chemical Society, 1983. "Principals of environmental analysis", Analytical Chemistry, 55: 2210-2218.

de Angelis, Marie A. and Marvin D. Lilley, 1987. "Methane in surface waters of Oregon estuaries and rivers," Limnology and Oceanography, 32(3), 716-722.

Bouck, Gerald R., 1982. "Gasometer: An inexpensive device for continuous monitoring of dissolved gases and supersaturation," Transactions of the American Fisheries Society, 111:505-516.

Ervine, D.A. and Elsawy, E.M. 1975. "The effect of a falling nappe on river aeration," Proceedings XVI Congress, Int'l. Association for Hydraulic Research, IAHR, Delft, The Netherlands, Vol. 3, 390-397.

Ervine, D.A. and Falvey, H.T. 1987. "Behavior of turbulent waterjets in the atmosphere and in plunge pools," Proceedings, Inst. of Civil Engineers, Vol. 83, No. 2, 295-314.

Gulliver, J.S., J.R. Thene, and A.J. Rindels, 1990. "Indexing gas transfer in self-aerated flows," ASCE, Journal of Environmental Engineering, 116(3), 503-523.

Gulliver, J. S. and S. C. Wilhelms, 1992. "Discussion of aeration at Ohio River Basin navigation dams," ASCE, Journal of Environmental Engineering, 118(3), 444-446.

Gulliver, J. S. and A. J. Rindels, 1993. "Measurement of air-water oxygen transfer at hydraulic structures," ASCE, Journal of Hydraulic Engineering, in press.

Hanratty, T. J., 1991. "Effect of gas flow on physical absorption," in Air-Water Mass Transfer, Wilhelms, S. C. and J. S. Gulliver, eds., ASCE, New York, NY, 10-13.

Johnson, P.L., 1984. "Prediction of dissolved gas transfer in spillway and outlet works stilling basin flows," in Gas Transfer at Water Surfaces, Brutsaert, W. and G. H. Jirka, eds., D. Reidel Publishing Company, Boston, MA, 605-612.

Lovley, D. R., F. Dwyer, and M. J. Klug, 1982. "Kinetic analysis of competition between sulfate reducers and methanogens for hydrogen in sediments," Applied and Environmental Microbiology, 43(6), 1373-1379.

McCutcheon, S. C., 1989. Water Quality Modeling, Vol. 1: Transport and Surface Exchange in Rivers, CRC Press, Boca Raton, FL, 336 pp.

McDonald, J. P. and J. S. Gulliver, 1992. Methane tracer technique for gas transfer at hydraulic structures, St. Anthony Falls Hydraulic Laboratory Project Report 325, University of Minnesota, Minneapolis, MN, 103 pp.

National Research Council, International Critical Tables, vol. III, McGraw-Hill, Inc., New York, 1929.

Rathbun, R.C., D.W. Stephens, D.J. Schultz, and D.Y. Tai, 1978. "Laboratory Studies of gas tracers for reaeration," Journal of Environmental Engineering Division, ASCE, 104(EE2), 1215-1220.

Rathbun, R. E., 1990. "Prediction of stream volatilization coefficients," ASCE, Jour. of Environmental Engineering, 116(3), 615-631.

Strayer, Richard F. and James M. Tiedge, 1978. "In situ methane production in a small, hypereutrophic, hard-water lake: Loss of methane from sediments by vertical diffusion and ebullition," Limnology and Oceanography, 28(6), 1201-1206.

Thene, J. R. and J. S. Gulliver, 1990. "Gas transfer measurements using headspace analysis of propane," Journal of Environmental Engineering, 116(6), 1107-1124.

Tsivoglou, E.C., 1968. "Tracer Measurement of Stream Reaeration: II. Field Studies," Journal of the Water Pollution Control Federation, 77(2), 219-262.

Weast, R.C., editor, 1976, Handbook of Chemistry and Physics 57th edition, CRC Press, Cleveland, Ohio.

Wetzel, R. G., 1975. Limnology, W. B. Sanders Co., Philadelphia, PA.

Wilhelms, S.C., J.S. Gulliver, and K. Parkhill, 1993. "Rearation at Low-Head Structures," Technical Report W-93-?, US Army Engineer Waterways Experiment Station, Vicksburg, MS.

Zeikus, J. G. and M. R. Winfrey, 1976. "Temperature limitation of methanogenesis in aquatic sediments," Applied and Environmental Microbiology, 31(2), 99-107.

Appendix I - Notation

A = air-water surface area
C = concentration in water
C_a = concentration in the air
C_b = time averaged methane concentration in a bubble
C_d = concentration downstream of the structure
C_m = concentration of methane in a bubble as it is released to the atmosphere
C_{me} = equilibrium concentration of methane in a bubble downstream of a structure
C_{N2} = dissolved nitrogen concentration
C_s = saturation concentration
C_{se} = effective saturation concentration
C_u = concentration upstream of the structure
$comp$ = molar fraction of gas in the atmosphere
D = diffusivity of the measured compound in the water
D_{eff} = effective bubble depth
D_O = diffusivity of oxygen in water
E = gas transfer efficiency
E_m = methane gas transfer efficiency
E_{iO} = equivalent transfer efficiency of oxygen
F = water surface flux of a volatile chemical per unit surface area
f_i = indexing parameter for chemical and temperature
f_g = indexing parameter for chemical
f_T = indexing parameter for temperature
H = Henry's Law constant
K_L = liquid film coefficient
K_p = conversion constant from atmospheres to depth of water
M = molecular weight of methane
P_{atm} = barometric pressure
P_{H2O} = vapor pressure of water
P_{N2} = partial pressure of nitrogen
P_{O2} = partial pressure of oxygen
q_a = specific air entrainment rate
q_w = specific flowrate of water
R = universal gas constant
t = residence time
T = water temperature
V = control volume over which A and C are measured
V_a = volume of headspace in a sample bottle
V_w = volume of water in a sample bottle

Appendix II - Air Entrainment Data

q_{air} measured at the Rum River Dam 2/17/90
q_{water} = 108 cfm/ft

Distance from plunge point (ft)	Run #1 q_{air} (cfm/ft)	Run #2 q_{air} (cfm/ft)
0.75	6.47	9.53
2.25	7.27	5.73
3.75	3.40	4.20
5.25	8.00	6.47
6.75	2.67	4.20
8.25	4.93	4.93
9.75	7.27	6.47
11.25	4.20	4.93
12.75	2.67	3.40
14.25	2.00	4.20
15.75	1.40	2.00
17.25	0.80	0.80
18.75	0	0
total q_{air}	76.62	85.29

Appendix III - Description of Structures

Kost Dam

The Kost Dam is located on the Sunrise River in Chisago County, Minnesota. The dam consists of an ungated ogee spillway. A plan view and a profile view of the dam are shown in Figs. 13 and 14, respectively.

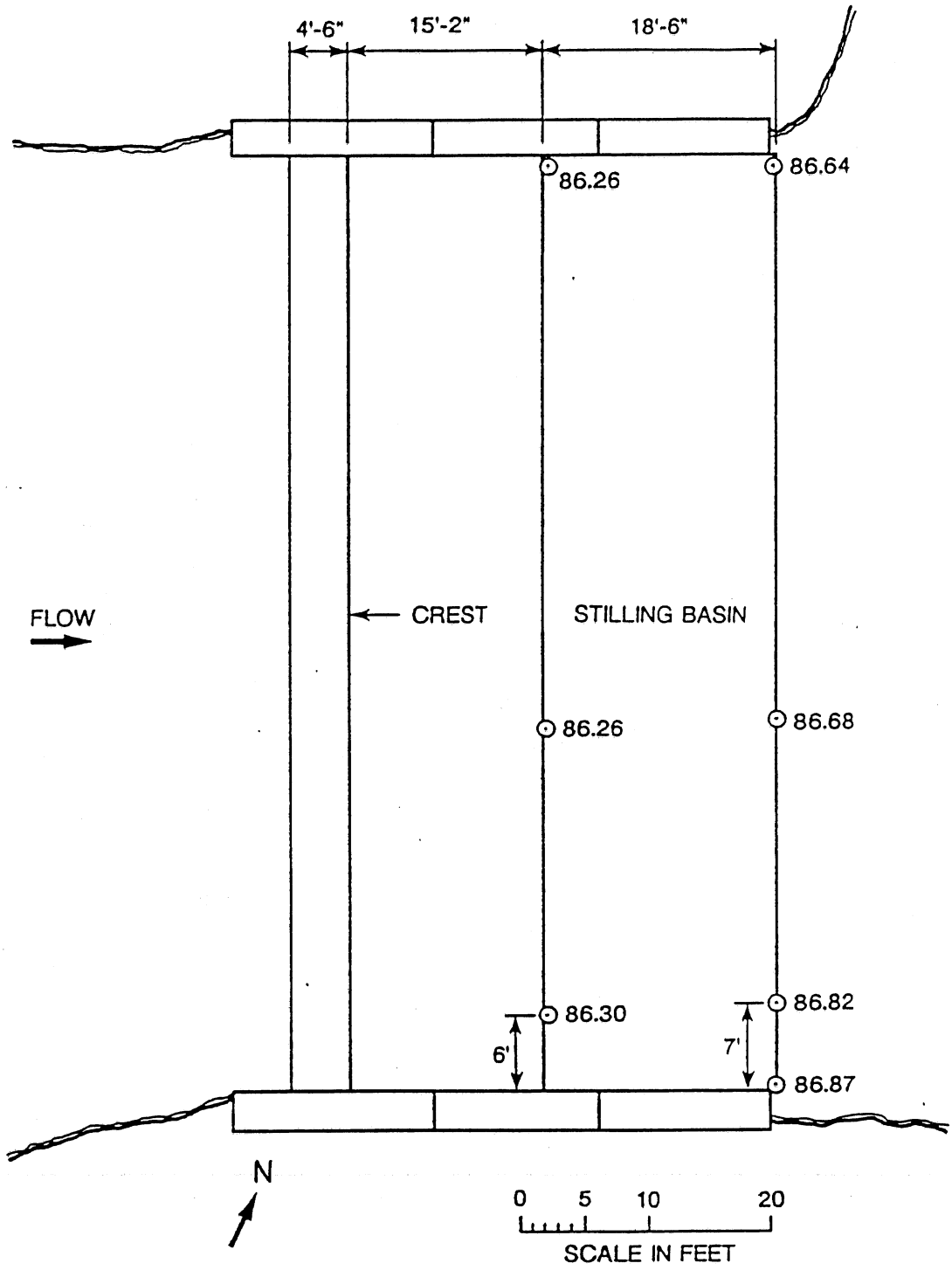

Figure 13 - Plan view of Kost Dam

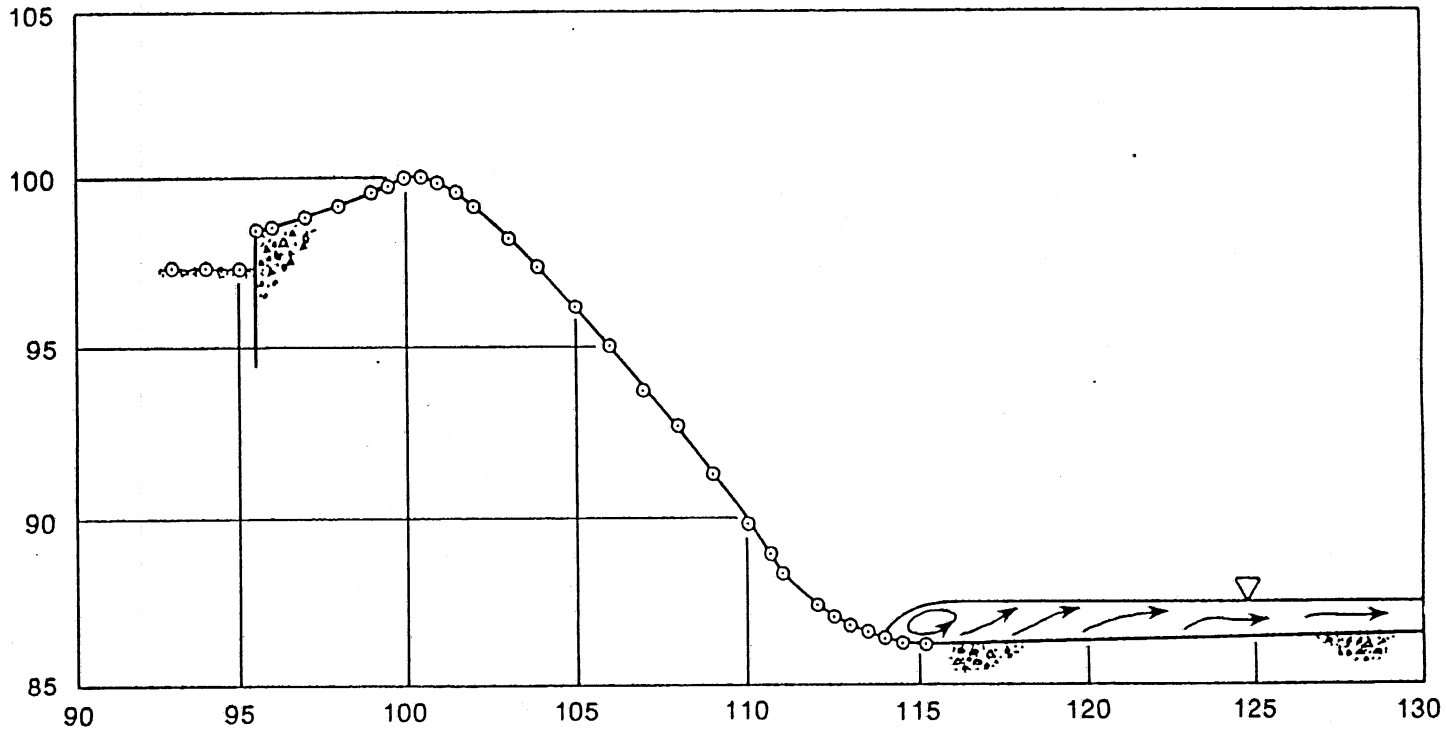

Figure 14 - Profile view of Kost Dam

Rum River Dam

The Rum River Dam is located on the Rum River, approximately 500 feet upstream of the Main Street Bridge in Anoka, Minnesota. The structure consists of a 236 foot long fixed weir, and a 20 foot wide tainter gate. The tainter gate spillway is separated from the main river by a concrete pier. The plan view of the structure and the specific sampling locations are shown in Fig. 15. The profile of the fixed weir is shown in Fig. 16. The profile of the tainter gate and spillway is shown in Fig. 17.

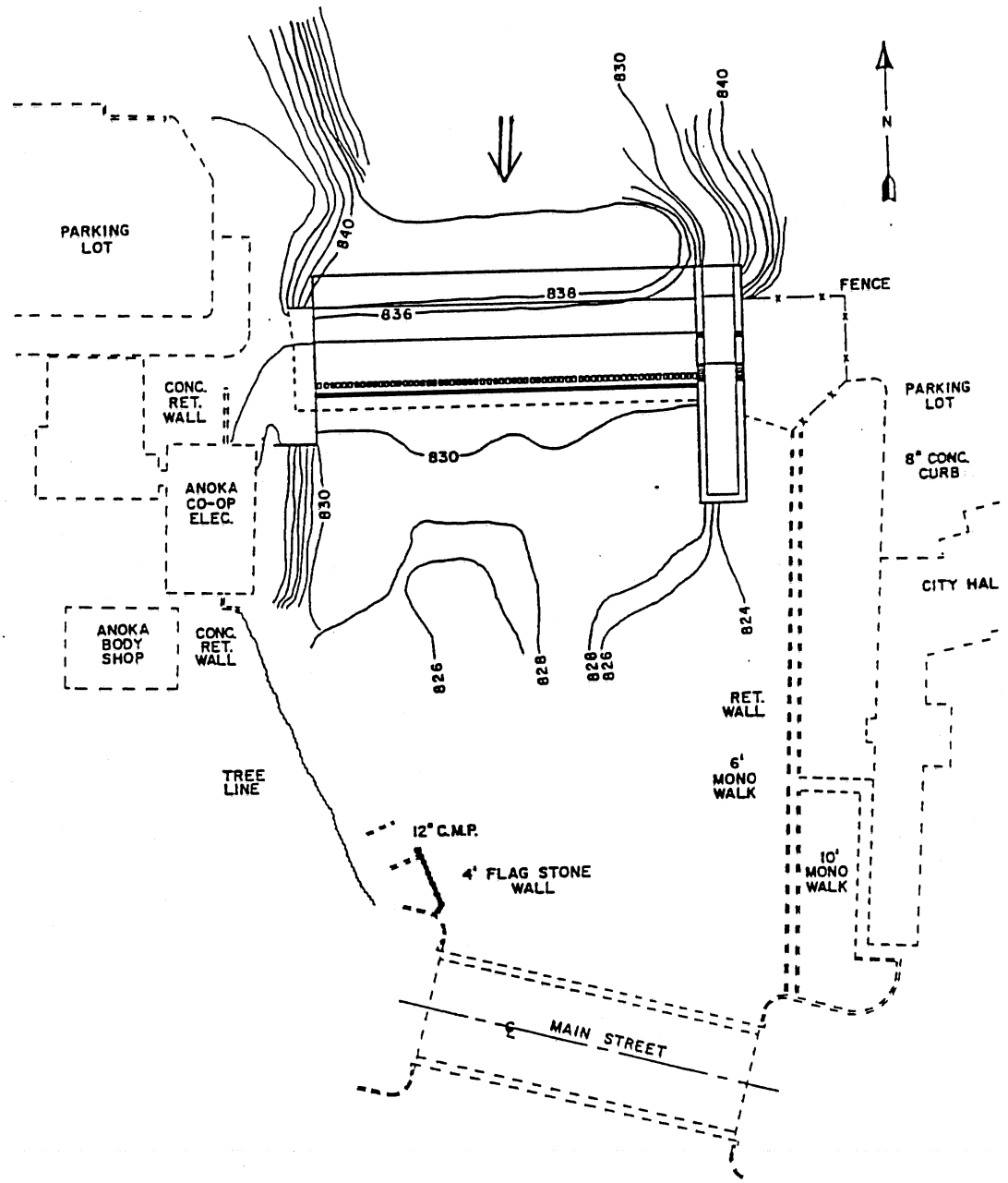

Figure 15 - Plan view of Rum River Dam

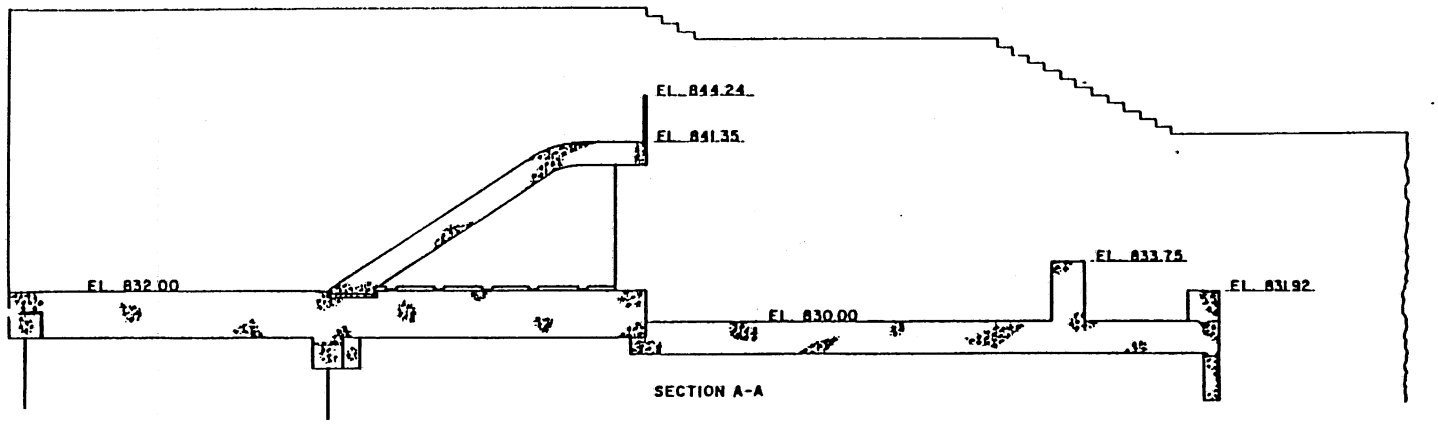

Figure 16 - Profile of Rum River fixed weir

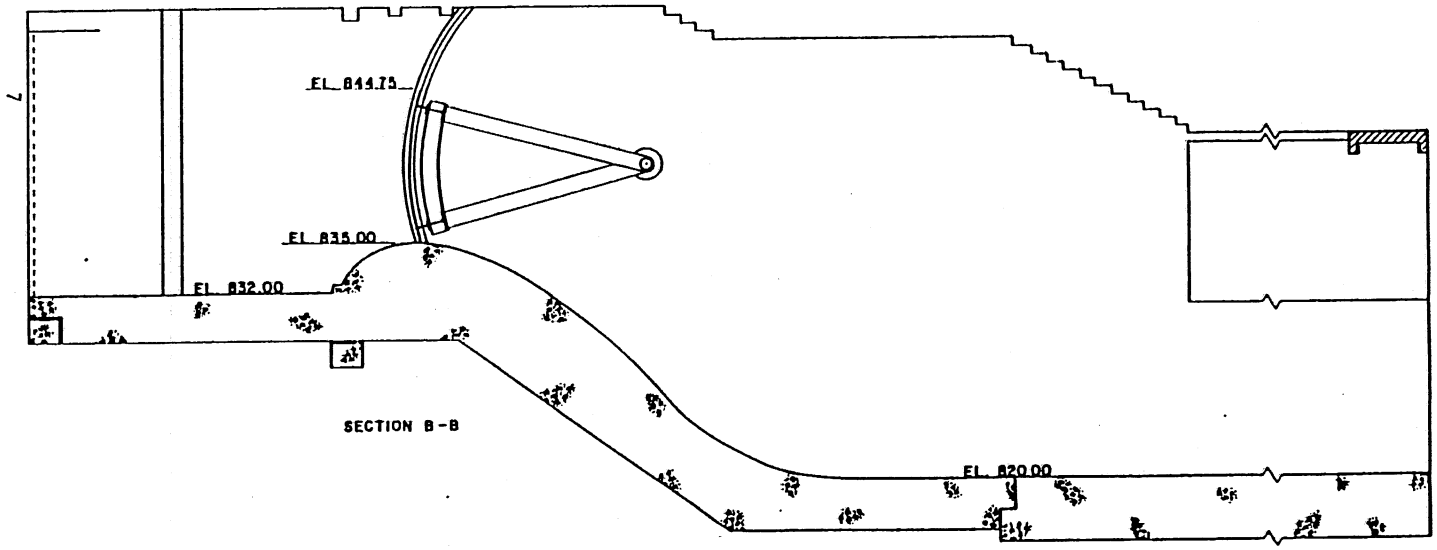

Figure 17 - Profile of Rum River tainter gate

St. Cloud Dam

The St. Cloud Dam is located on the Mississippi River approximately 500 feet downstream of the 10th Street Bridge in St. Cloud Minnesota. The structure consists of a 500 foot long fixed weir, and two tainter gates. The tainter gate spillway is separated from the main river by a concrete pier. The plan view of the structure and the sampling locations are shown in Fig. 18. Only the tainter gate portion of the structure was investigated in this study. The profile of the tainter gate and spillway is shown in Fig. 19.

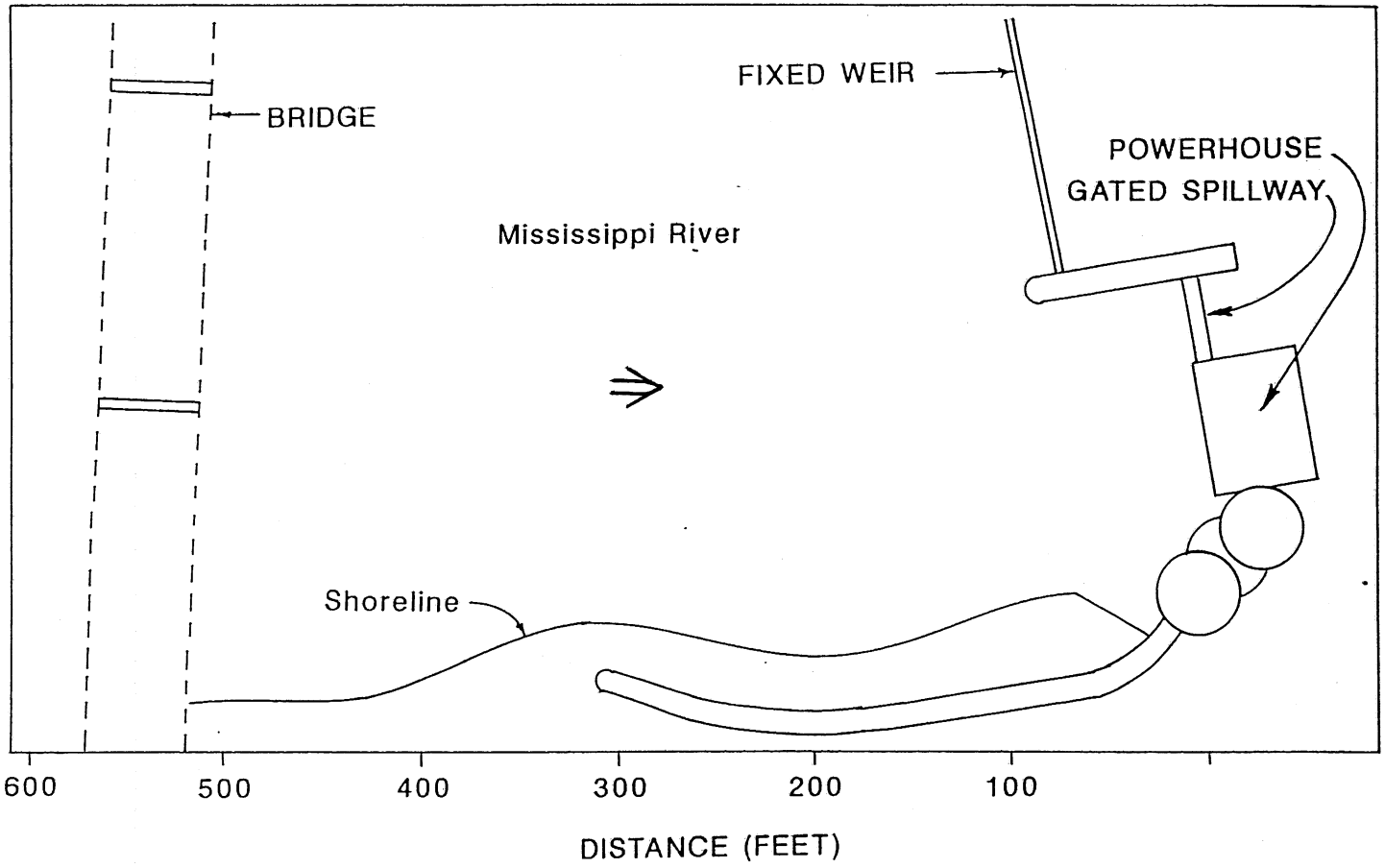

Figure 18 - Plan view of St. Cloud Dam

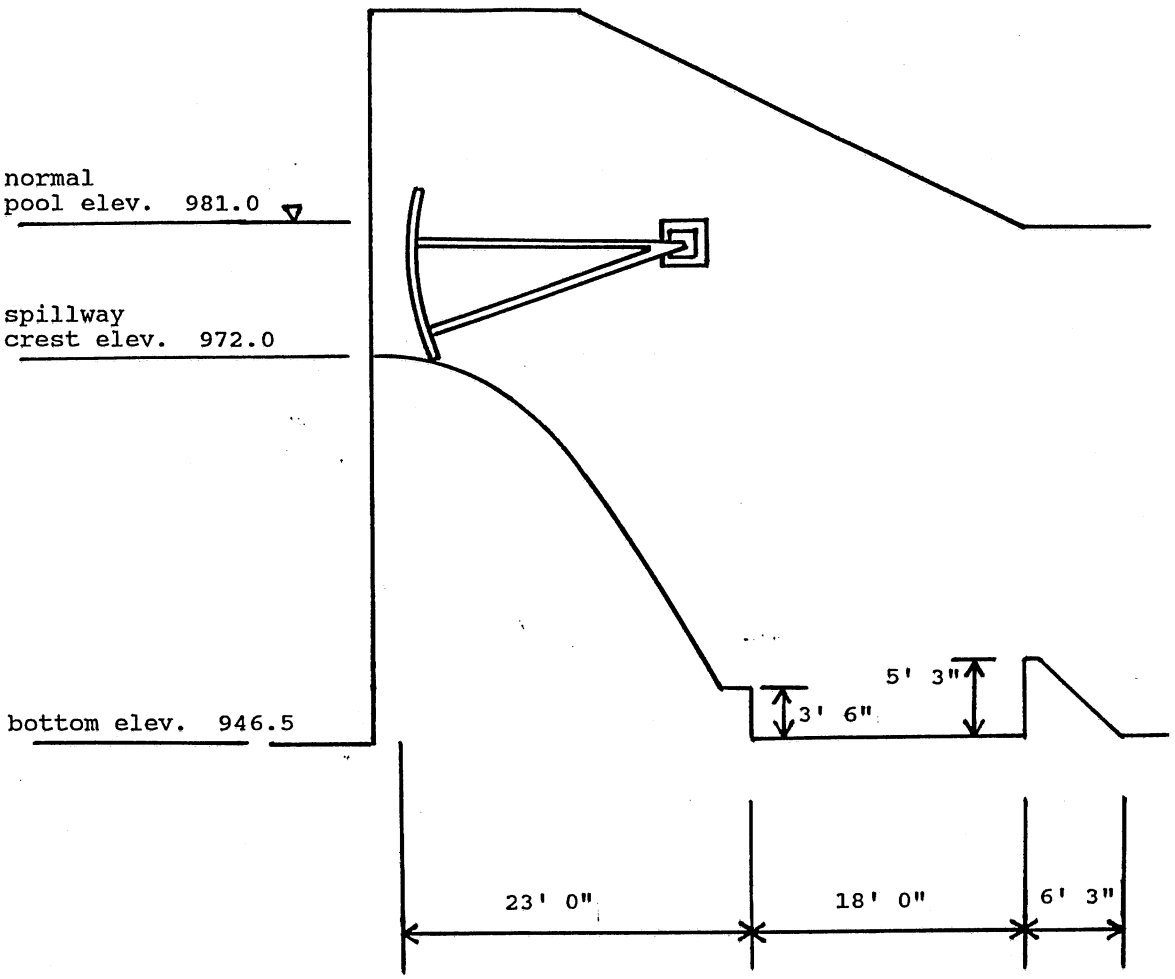

Figure 19 - Profile view of St. Cloud Dam

Smithland Lock and Dam

The Smithland Lock and Dam is located on the Ohio River near Paducah, Kentucky. A profile of the dam is shown in Fig. 20.

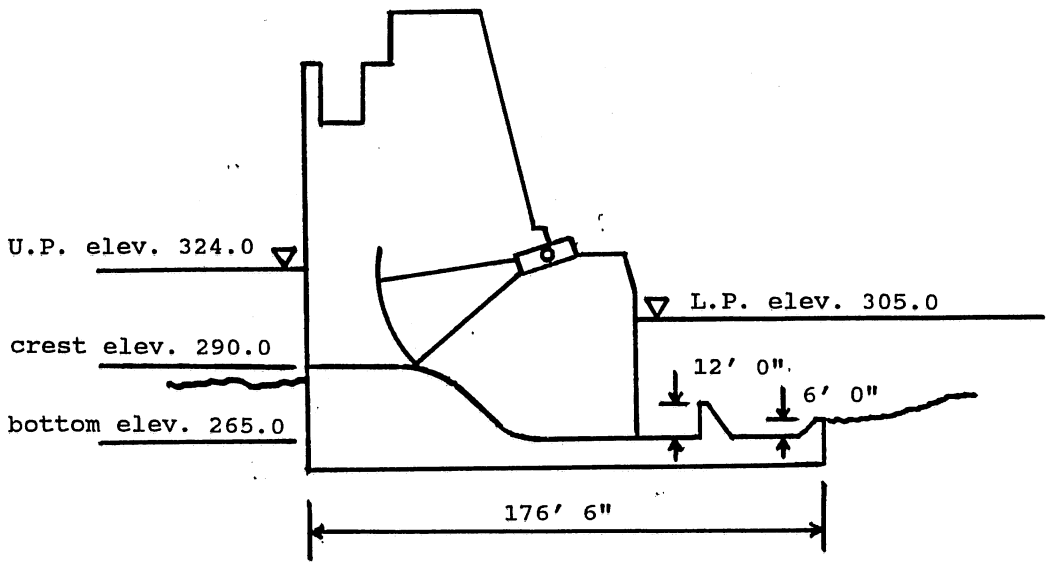

Figure 20 - Profile view of Smithland Lock and Dam

Opekiska Lock and Dam

The Opekiska Lock and Dam is located on the Monogahelia River near Morgantown, West Virginia. A profile of the dam is shown in Fig. 21.

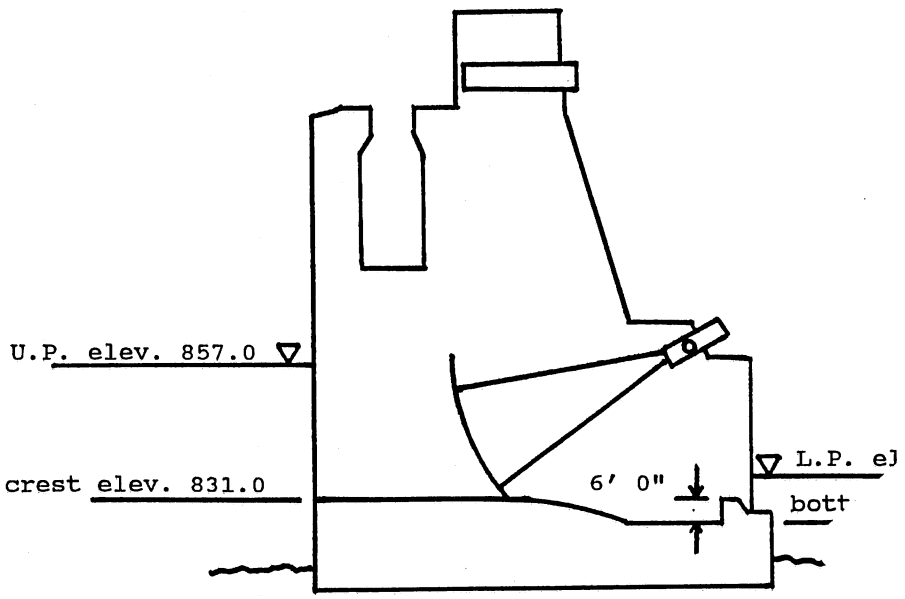

Figure 21 - Profile view of Opekiska Lock and Dam